

The Pennsylvania State University
The Graduate School
Department of Mechanical and Nuclear Engineering

**EFFECTS OF BLOCKAGES ON THE EFFECTIVENESS OF
CYLINDRICAL FILM COOLING HOLES**

A Thesis in
Mechanical Engineering
by
Christopher A. Whitfield

© 2013 Christopher A. Whitfield

Submitted in Partial Fulfillment
of the Requirements
for the Degree of

Master of Science

December 2013

The thesis of Christopher A. Whitfield was reviewed and approved* by the following:

Karen A. Thole
Head of the Department of Mechanical and Nuclear Engineering
Professor of Mechanical Engineering
Thesis Advisor

Daniel C. Haworth
Professor-In-Charge of MNE Graduate Programs
Professor of Mechanical Engineering

Savas Yavuzkurt
Professor of Mechanical Engineering

*Signatures are on file in the Graduate School

Abstract

As power and efficiency demands for gas turbines increase, turbine inlet temperatures are rising. Gas turbine designers use various technologies to help keep turbine hardware cool. Among these technologies are film cooling and thermal barrier coatings (TBCs). These two technologies impact one another, as coatings on the blades may block film cooling holes. Few studies have investigated the effect of spraying the TBC across the airfoil on film cooling performance. The focus of this study was to evaluate the detrimental effects of blocked holes resulting from TBC spray on a film cooled airfoil.

A process was developed to spray a blockage representative of what would occur along an actual airfoil. A nozzle was constructed that atomized insulating foam such that the foam could be sprayed on top of film cooling holes in a line-of-sight manner. Adiabatic effectiveness measurements, representative of the cooling performance, were taken for unblocked cylindrical holes as well as blocked holes. Measurements were performed on a row of five cylindrical film cooling holes at an inclination angle of 30 degrees and a pitchwise spacing of $P/D = 6.7$ for blowing ratios between $M = 0.5$ and $M = 1.0$. The blockages were found to decrease the adiabatic effectiveness of cylindrical holes up to 70% at a blowing ratio of $M = 1.0$ relative to unblocked holes. The reduction in the cooling benefit scaled with the ratio of the coolant jet to mainstream momentum flux evaluated at the exit of the hole.

Table of Contents

List of Figures	v
List of Tables	vii
Nomenclature	viii
Acknowledgements.....	x
Chapter 1 Introduction	1
1.1 Introduction to Film Cooling	2
1.2 Thermal Barrier Coatings and Their Impact on Airfoil Cooling.....	4
1.3 Objectives.....	6
Chapter 2 Review of Previous Studies.....	7
Chapter 3 Experimental Facility and Methods	10
2.1 Uncertainty Analysis.....	16
Chapter 4 Effects of Blockages on Film Cooling Holes	18
4.1 Blockage Effects on Discharge Coefficient	18
4.2 Blockage Effects on Adiabatic Effectiveness	20
4.3 Scaling the Reduction in Adiabatic Effectiveness Due to Blockage.....	30
Chapter 5 Conclusions	34
5.1 Recommendations for Future Work.....	35
References.....	37
Appendix Uncertainty Analysis.....	39
A.1. Uncertainty in Flow Quantities	39
A.2. Uncertainty in Adiabatic Effectiveness.....	42

List of Figures

Figure 1-1. Advancements in turbine cooling technology with the corresponding increase in turbine entry temperature [1]	2
Figure 1-2. Schematic of a film cooling hole (a) without and (b) with a TBC coating applied.....	5
Figure 2-1. A micrograph of a blocked film cooling hole [6].....	9
Figure 3-1. Schematic of wind tunnel used in the current study.....	11
Figure 3-2. Schematic of the test section.	12
Figure 3-3. (a) Schematic and (b) photograph of nozzle for atomizing and spraying foam	13
Figure 3-4. Photograph looking into a cylindrical hole with a $t/D=0.5$ blockage.....	14
Figure 3-5. A cross-sectional photograph of a sprayed hole.....	14
Figure 3-6. A sample $DR = 1.5$ calibration curve.....	16
Figure 4-1. Discharge coefficients for cylindrical holes.....	19
Figure 4-2. Discharge coefficients for unblocked and blocked holes.....	19
Figure 4-3. Laterally averaged effectiveness results at $M = 0.5$ and $M = 1.0$	20
Figure 4-4. Centerline effectiveness results at $M = 0.5$	21
Figure 4-5. Cylindrical hole adiabatic effectiveness contours for $DR=1.5$ $M=0.5$: (a) unblocked hole, (b) blocked hole with matched PR, and (c) blocked hole with matched M.....	24
Figure 4-6. Cylindrical hole adiabatic effectiveness contours for $DR=1.2$ $M=0.5$: (a) unblocked hole, (b) blocked hole with matched PR, and (c) blocked hole with matched M.....	24
Figure 4-7. (a) Centerline and (b) laterally averaged effectiveness at $M = 0.5$, $DR = 1.5$	25
Figure 4-8. Cylindrical hole adiabatic effectiveness contours for $DR=1.5$ $M=0.75$: (a) unblocked hole, (b) blocked hole with matched PR, and (c) blocked hole with matched M.....	26

Figure 4-9. Cylindrical hole adiabatic effectiveness contours for $DR=1.2$ $M=0.75$: (a) unblocked hole, (b) blocked hole with matched PR, and (c) blocked hole with matched M.....	26
Figure 4-10. (a) Centerline and (b) laterally averaged effectiveness at $M = 0.75$, $DR = 1.5$	27
Figure 4-11. Cylindrical hole adiabatic effectiveness contours for $DR=1.5$ $M=1$: (a) unblocked hole, (b) blocked hole with matched PR, and (c) blocked hole with matched M.....	28
Figure 4-12. Cylindrical hole adiabatic effectiveness contours for $DR=1.2$ $M=1.0$: (a) unblocked hole, (b) blocked hole with matched PR, and (c) blocked hole with matched M.....	29
Figure 4-13. (a) Centerline and (b) laterally averaged effectiveness at $M = 1.0$, $DR = 1.2$	29
Figure 4-14. Area averaged effectiveness plotted against (a) blowing ratio and (b) effective momentum flux ratio.....	32
Figure 4-15. Percent change in area averaged effectiveness plotted against the effective momentum flux of the blocked hole.	33

List of Tables

Table 3-1. Boundary Layer Characteristics [15].....	10
Table 3-2. Description of Cylindrical Holes.....	12
Table 3-3. Configurations of Simulated TBC Coating Tested.....	15
Figure 3-5. A sample DR = 1.5 calibration curve.....	16
Table 4-1. Comparison of Geometry and Flow Conditions for Cylindrical Holes.....	21
Table 4-2. Blowing and Momentum Flux Ratios Tested in the Current Study.....	22
Table A-1. Uncertainty Progression [22].....	40
Table A-2. Bias, Precision, and Total Uncertainties for Measured and Calculated Quantities at $M = 1.0$	41
Table A-3. Bias, Precision, and Total Uncertainties for Measured and Calculated Quantities at $M = 0.5$	41
Table A-4. Uncertainties for Adiabatic Effectiveness at DR = 1.5.....	43
Table A-5. Uncertainties for Adiabatic Effectiveness at DR = 1.2.....	43

Nomenclature

A	hole cross-sectional area
AR	area ratio
c	length of flattened spray
D	diameter of film-cooling holes
DR	density ratio
I	momentum flux ratio
L	injection hole length
M	blowing ratio
P	lateral distance between holes, pitch
PR	pressure ratio
t	coating thickness
T	temperature
TBC	thermal barrier coating
U	velocity
VR	velocity ratio
w	breakout width of the hole
x	streamwise distance measured from the unblocked hole downstream edge
y	vertical distance measured from the wall surface
z	lateral distance in the pitchwise direction

Greek

α	injection angle
δ	99% boundary layer thickness
η	adiabatic effectiveness
θ	momentum thickness
ρ	fluid density

Subscripts

aw	adiabatic wall
b	blocked
c	coolant
CL	centerline
eff	effective, at the hole exit
exit	evaluated at the hole exit
hole	across the hole
inlet	evaluated at the inlet of the hole
t	total
ub	unblocked
w	wall
∞	freestream

Superscripts

-	laterally-average value
=	area-averaged value

Acknowledgements

I would first like to thank Dr. Karen Thole, my adviser, for bringing me on as an undergraduate, encouraging me to go on to grad school, having high expectations once I decided to stay on for a Master's, and for being reasonable and supportive the entire time. She was a fantastic adviser, and genuinely enthusiastic about everything that I was working on. I also want to thank Robert Schroeder for helping with experiments and allowing me to ask him questions whenever and wherever they come up. Robert was an invaluable resource to me for this project. Even though she graduated a year before me, I need to thank Molly Eberly for teaching me the ins and outs of the rig, and being patient with me when I made mistakes. I want to thank the other members of the lab that I did not work directly with, but were nonetheless vital for me to ask questions to, joke around with, eat lunch with and share late nights working/doing homework: Amy, Katie, Jeff, Curtis, Ken, Shane, Cory, Jake, Andrew, Mike L. and Mike B. This work would not be possible without financial and technical support from Pratt and Whitney, particularly Scott Lewis, Atul Kohli, Mark Zelesky and Dominic Mongollo.

Last but certainly not least, I want to thank my friends and family in Arizona for supporting me from 2,000 miles away. They know how to put things in perspective during an especially busy week. I want to thank my parents especially for letting me choose my own path, they did not pressure me to do anything, but rather let me make my own decisions.

Chapter 1

Introduction

Gas turbines are commonly used in power generation and aircraft propulsion applications. Increasing the efficiency of these engines is of particular importance due to rising fuel costs and increased emissions regulations. Increasing pressure ratios increase the thermal efficiency of a gas turbine, but also increase the turbine inlet temperature. The turbine inlet temperature of a modern gas turbine is higher than the melting temperature of the components, requiring the use of cooling air to keep the components such as airfoils from melting. Coolant air for the turbine components come from compressor bleed air that is bypassed around the combustor. This coolant air does no useful work and reduces the overall thermal efficiency of the engine. It is in the interest of the turbine designer to use coolant air as efficiently as possible to minimize the parasitic drain on the engine by using compressor air to cool the hardware. The increase in turbine inlet temperature with various cooling technologies is shown in Figure 1-1.

Cooling of turbine hardware is done in a variety of ways. The internal surfaces are cooled using turbulators, impingement jets, and pin fins, for example [1]. External surfaces are cooled mainly through the use of film cooling. In film cooling, coolant air in a turbine blade, vane, or endwall is routed through small holes in the airfoil surfaces before exiting into the hot gas path. This coolant air creates a film of cool air in between the external surface of the hardware and the hot gas path. This film of cool air effectively reduces the driving temperature difference for convection, this reducing the heat flux on the surface of turbine hardware.

Another technology for reducing the heat flux into turbine hardware is to coat the surfaces with an insulating material, which is known as a thermal barrier coating (TBC). A TBC is a ceramic coating applied to surfaces along the hot gas path. Film cooling holes are typically machined in the metal before the protective coating is applied. TBCs are usually applied using an air-plasma spray (APS) or electron beam-physical vapor deposition (EB-PVD) process [2]. In both processes, the TBC can deposit into film cooling holes, altering the holes from their initial design specifications. These deposits are effective blockages for the flow coming out of film cooling holes.

The interaction between these two technologies has not been very well investigated. Little work has been done to determine the effect of blockages on film cooling flows. This thesis presents film effectiveness for widely spaced cylindrical holes both unblocked and with a representative TBC blockage.

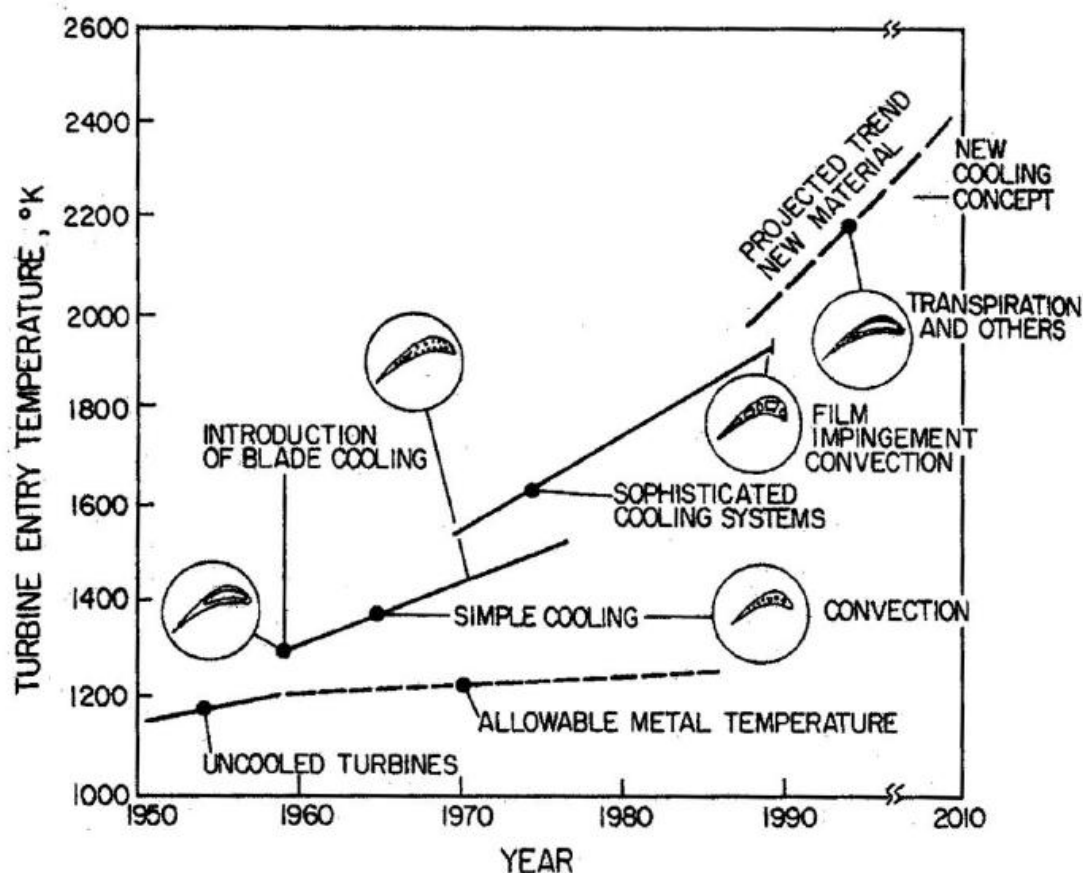


Figure 1-1. Advancements in turbine cooling technology with the corresponding increase in turbine entry temperature [1].

1.1 Introduction to Film Cooling

Meaningful film cooling experiments match the non-dimensional parameters to that of an actual engine. These non-dimensional parameters, such as the density ratio, velocity ratio, mass flux ratio, momentum flux ratio and adiabatic effectiveness, have been defined by Pederson et al. [3]. Film cooling flowfields are complex, as they are governed the coolant flow and the

mainstream flow. The density ratio (DR), given by equation 1-1, is the ratio of the coolant flow density to the mainstream flow density. Because of the large difference in temperature between the two flows in an engine, this ratio is typically between 1.5 and 2.0.

$$DR = \frac{\rho_c}{\rho_\infty} \quad (1-1)$$

The velocity ratio (VR) is the ratio of coolant flow velocity to mainstream flow velocity, and is given by equation 1-2 [3].

$$VR = \frac{U_c}{U_\infty} \quad (1-2)$$

The mass flux or blowing ratio (M) is defined as the product of the density ratio and velocity ratio. The blowing ratio allows the turbine designer to, along with the cross sectional area of a film cooling hole, calculate the mass flow through the hole. The blowing ratio is shown in equation 1-3.

$$M = DR * VR = \frac{\rho_c U_c}{\rho_\infty U_\infty} \quad (1-3)$$

The momentum flux ratio is the ratio of momentum flux in the coolant jet to the momentum flux in the mainstream [3]. This ratio is of particular importance for cylindrical film cooling holes. The momentum flux ratio is the non-dimensional parameter that best describes jet detachment. Jet detachment occurs when the momentum of the coolant jet is large enough relative to the momentum of the mainstream flow such that the coolant jet separates from the surface it is intended to cool. The momentum flux ratio is given by equation 1-4.

$$I = DR * VR^2 = \frac{\rho_c U_c^2}{\rho_\infty U_\infty^2} \quad (1-4)$$

This jet detachment lowers the film effectiveness, η , which is defined by equation 1-5 [3],

$$\eta = \frac{T_\infty - T_{aw}}{T_\infty - T_c} \quad (1-5)$$

where T_∞ is the mainstream temperature, T_{aw} is the temperature of the fluid just at the wall, and T_c is the temperature of the fluid in the film cooling hole. η is a local quantity, and varies between unity and zero. The film effectiveness describes the amount of coolant that is attached to the surface.

1.2 Thermal Barrier Coatings and Their Impact on Airfoil Cooling

Thermal barrier coatings (TBCs) are another way of reducing the heat flux into turbine components. A TBC is simply an insulating layer of low conductivity material coating the airfoil, which is made from single-crystal casting. TBCs are typically sprayed on an airfoil with an air-plasma spray (APS) or electron beam-physical vapor deposition (EB-PVD) process [2]. These coatings are often applied after film cooling holes have been machined into the base metal, and thus some of the coating will deposit into the film cooling holes. The way in which the coating deposits in the film cooling holes is related to the application process. Experiments in this thesis simulate a TBC coating applied in a line-of-sight manner, which both APS and EB-PVD processes use. There has been very little work on characterizing the effect of TBC blockages on film cooling.

While there are hundreds of different film cooling hole geometries in the open literature, experiments in this thesis were all performed with cylindrical holes. Cylindrical holes have been studied quite extensively, are still used today, and provide a good baseline to characterize the effects of TBC coatings on film cooling.

TBC depositing into film cooling holes creates a blockage that decreases the outlet area for coolant air. Figure 1-2 shows a schematic of a cylindrical film cooling hole. Figure 1-2a shows an unblocked hole with inlet area A_{in} and outlet area $A_{out,ub}$. Across the hole, the hole has an unblocked area ratio, AR , defined by equation 1-6.

$$AR = \frac{A_{out,ub}}{A_{in}} \quad (1-6)$$

By definition, an unblocked cylindrical hole has an area ratio of unity. Figure 1-2b shows a blocked hole with the same inlet area, but a different outlet area. This outlet area, $A_{out,b}$, is always smaller than $A_{out,ub}$. This leads to a different area ratio, an effective area ratio due to blockage, or AR_{eff} .

$$AR_{eff} = \frac{A_{out,b}}{A_{in}} \quad (1-7)$$

AR_{eff} for cylindrical holes is always less than unity. This negatively affects film cooling performance because it increases the exiting jet momentum thereby increasing the likelihood of jet separation. Because of the potentially large changes in outlet area, the momentum flux ratio simply based on the hole diameter can be misleading. As a part of this research, a new

momentum flux ratio was defined using the hole exit area, which is more meaningful when holes are blocked. The effective momentum flux, evaluated at the exit of the hole, is given in equation 1-8.

$$I_{\text{eff}} = \frac{\rho_c U_{c,\text{exit}}^2}{\rho_\infty U_\infty^2} = \frac{I}{AR_{\text{eff}}^2} \quad (1-8)$$

As will be described later in this thesis, I_{eff} is used to help scale the reductions in film cooling effectiveness as a result of blockage.

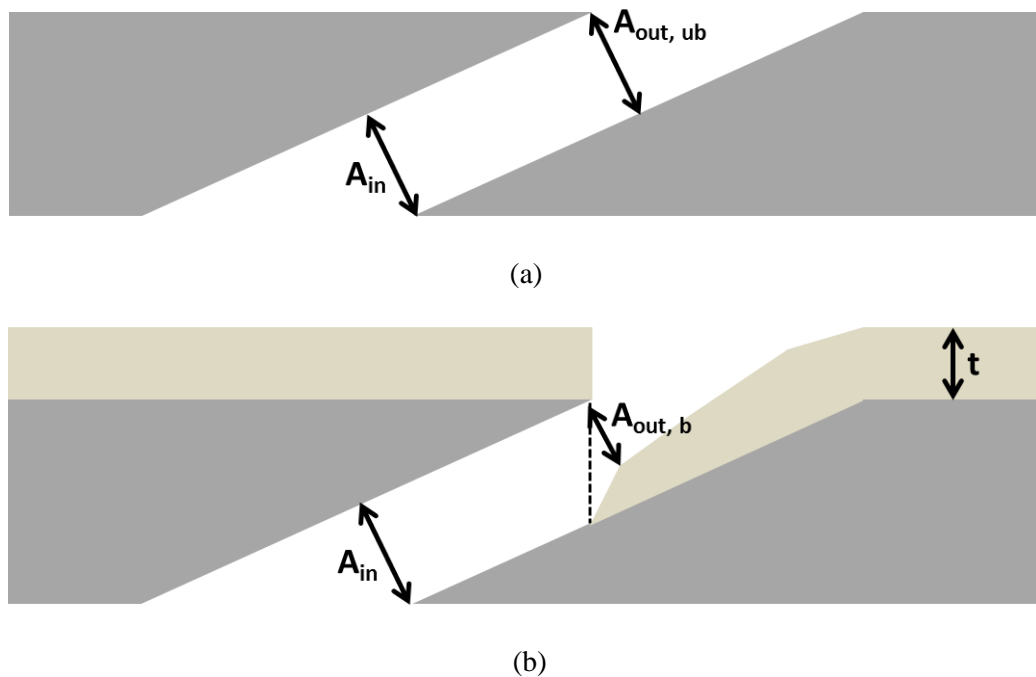


Figure 1-2. Schematic of a film cooling hole (a) without and (b) with a TBC coating applied

Another effect of blockages in film cooling holes is a drop in flowrate across the hole. Blockages lower the flow exit area, which in turn lowers the amount of coolant that can flow through the holes. The discharge coefficient measures the ratio of the mass flow that actually occurs to the ideal frictionless mass flow, and is given by equation 1-9.

$$C_d = \frac{\dot{m}_{\text{actual}}}{\dot{m}_{\text{ideal}}} = \frac{\dot{m}_{\text{actual}}}{A_{\text{hole}} \sqrt{2\rho_c * \Delta P_{\text{holes}}}} \quad (1-9)$$

Equation 1-9 is for incompressible flows only. The area (A_{hole}) used in the calculation will be defined two different ways: the first is the inlet area of the hole, and the second is the minimum (metering) flow area found anywhere in the hole. Typically, the discharge coefficient is measured using the minimum flow area, which would ordinarily be sufficient, but in blocked film cooling holes, the minimum flow area is not always known. Thus, the discharge coefficient defined by the inlet area of the hole is most useful to gas turbine designers. The inlet area of the hole is always known, and most other flow properties are defined using the inlet area of the holes.

In an actual gas turbine engine, film cooling holes do not have a constant flowrate but rather a constant pressure ratio. The pressure ratio across the hole drives the coolant flowing through the hole. To simulate engine conditions, film cooling experiments must match the pressure ratio across the holes instead of the mass flux ratio. In the current study, the mass flux ratio and the pressure ratio across the hole were matched for comparison.

1.3 Objectives

This thesis will investigate the effect of blockages in cylindrical film cooling holes. In Chapter 2, available literature about cylindrical film cooling holes and blockage effects on film cooling will be reviewed. Then, a description of the test facility, the methods used to block holes with a representative sprayed blockage, and the method used for testing the adiabatic effectiveness will be given in Chapter 3. Chapter 4 will present measured discharge coefficients as well as adiabatic effectiveness results for unblocked and blocked holes. The results will then be scaled using the effective momentum flux ratio, which was found to be the most meaningful scaling parameter.

Chapter 2

Review of Previous Studies

Film cooling is a widely studied technology, with many studies investigating the effects of blowing ratio, velocity ratio, momentum flux ratio, and hole geometry on film cooling holes. This study will focus on cylindrical hole geometries, but there are many studies in the available literature investigating shaped holes. Cylindrical holes, which are used in modern gas turbines, are a common baseline hole to understand the physics of film cooling. Sinha et al. [4] measured the adiabatic effectiveness for cylindrical holes at a variety of flow conditions. They found that the centerline effectiveness scaled with blowing ratio, but only for attached jets. They also found that laterally averaged effectiveness was dependent on the momentum flux ratio. High momentum flux ratios were found to have less effective cooling as a result of jet separation, leading to lower laterally averaged effectiveness. The highest laterally averaged effectiveness found by Sinha et al. was at $M = 0.5$.

Thole et al. [5] measured the temperature field downstream of cylindrical film cooling holes. They found that jet detachment scaled with the momentum flux ratio. They determined that jets with a momentum flux ratio, $I < 0.4$, were attached to the surface. Detached-then-reattached jets were observed from $0.4 < I < 0.8$, and for $I > 0.8$, jets were found to be completely detached.

The influence of density ratio on film cooling was first studied by Pederson et al. [3]. Instead of cryogenic cooling of the coolant flow to achieve engine realistic density ratios, the study made use of the heat- mass transfer analogy. A foreign gas was used as coolant to achieve large density ratios. Lateral spreading of the coolant jet was found to increase as the density ratio increased. Similar results were found by Sinha et al. [4] and Thole et al. [5]. It is worth noting, at a fixed mass flux ratio, an increase in density ratio will lead to a decrease in momentum flux ratio. A lower momentum flux ratio decreases the likelihood of jet detachment, which is beneficial to film cooling effectiveness.

All studies mentioned previously used pristine holes as manufactured. Pristine holes are not observed in an actual engine for a variety of reasons including deposition of foreign material, manufacturing effects and TBC sprays. Bogard et al. [6] showed the cross section of a film cooling hole with a blockage due to particle deposition (Figure 2-1). Figure 2-1 is a micrograph

of a cross section of a film cooling hole in a military aero-engine after more than 500 hours of use.

Experimental studies have shown the detrimental effects on adiabatic effectiveness of in-hole blockages in cylindrical film cooling holes. Jovanovic et al. [7] studied the impact of imperfections in manufacturing on film cooling holes. Laser drilling, a common process for manufacturing film cooling holes, commonly leaves deposits inside holes which is known as melt ejection. Jovanovic et al. found significant changes in the flowfield of a cylindrical hole blocked due to a half torus, which was used to model the melt ejections. Particle image velocimetry results showed large changes in the flowfield between pristine holes and blocked holes. Significant decreases in film cooling effectiveness were also found, with the decreases being larger at low velocity ratios. The half torus shape used in the study by Jovanovic et al. differs from that of sprayed blockages. Sprayed blockages occur directly below the breakout of a film cooling hole, whereas melt ejection can occur on all sides of a hole.

Demling and Bogard [8] investigated the effects of obstructions upstream, downstream and inside of film cooling holes. An obstruction half a hole diameter in height was placed at the hole leading edge, the hole trailing edge, and inside cooling holes on the suction side of a vane. They saw decreases in adiabatic effectiveness of up to 80% compared to unblocked holes for blockages placed inside the holes and on the leading edge of the hole. Obstructions placed at the trailing edge of the holes were found to have little effect on the film effectiveness. Demling [9] tested an additional in-hole obstruction that was a quarter of a hole diameter in height, which also caused a decrease in film effectiveness, though not as severe as the larger obstruction.

An investigation of in-hole deposition due to fuel contaminants was performed by Sundaram and Thole [10] for an endwall application. Blockages placed inside cylindrical film cooling holes were a thickness of $t/D = 0.3$ such that the exit area of the holes was reduced by 25%. In a row of five film cooling holes on a vane endwall, experiments were performed with one, two and all five holes blocked. They found that the laterally averaged effectiveness increased relative to an unblocked hole at the leading edge of the hole, then quickly decreased due to the blockages. Blocking one hole in the row of five was found to decrease the laterally averaged effectiveness by about 20%. Blocking all five holes was found to decrease the laterally averaged effectiveness by about 50% relative to unblocked holes.

Computational studies have studied the effects of a layer of TBC over top of a film cooling hole. Na et al. [11] ran simulations on a cylindrical hole with and without a layer of TBC over top. The layer of TBC was half a hole diameter thick, and experienced a sharp cutoff at the

leading edge of the hole. Na et al. found that blockages reduce the adiabatic effectiveness significantly when tested at the same blowing ratio. Larger decreases in effectiveness values were found for higher flowrates. This decrease was attributed to jet detachment due to the blockage. The blockage strengthened the counter-rotating vortex pair, which tends to lift the coolant jet off the surface.

Only two experimental studies to the authors' knowledge have examined the detrimental effects of a TBC coatdown on film cooling performance. Bunker [12] measured adiabatic film effectiveness for cylindrical and shaped holes with a TBC coating of $t/D=0.4$, sprayed using an APS process. He presented results only in terms of the centerline adiabatic effectiveness levels such that no information is known about the overall change in jet spreading. Bunker found that blockages resulted in a 50% reduction in centerline effectiveness at $M = 1$ for all $x/D < 50$ in cylindrical holes and a 30% reduction for all $x/D < 20$ in shaped holes at $M = 1$ and 1.2. Shaped hole centerline effectiveness recovered to unblocked values for shaped holes past $x/D = 40$.

Schroeder and Thole [13] analyzed over 130 different shaped holes in available literature and designed a baseline shaped hole that was characteristic of the many shaped holes found in the literature. This hole was a laidback fanshaped hole with conservative expansion angles of 7 degrees in the lateral and forward directions. Schroeder and Thole tested this hole at low and moderate freestream turbulence levels. The baseline shaped hole was also tested by Whitfield et al. [14] with blockages. Two blockages were tested inside the hole, one with a thickness of $t/D = 0.5$, the other with $t/D = 0.9$. Blockages resulted in a 75% decrease in film effectiveness for shaped holes. The decrease in effectiveness scaled with the effective momentum flux ratio for the shaped hole.

The results presented in this thesis are unique because the data includes spatially-resolved adiabatic effectiveness measurements for blocked cylindrical film cooling holes. Both centerline and laterally averaged adiabatic effectiveness values will be reported. This thesis also provides a method for scaling the blockage effects.



Figure 2-1. A micrograph of a blocked film cooling hole [6].

Chapter 3

Experimental Facility and Methods

All adiabatic effectiveness measurements were taken in a closed-loop wind tunnel shown in Figure 3-1 that was previously described by Eberly and Thole [15]. A schematic of the test section is shown in Figure 3-2. Mainstream air was circulated at 10 m/s by an in-line centrifugal fan. The mainstream air was thermally conditioned by a 1.4kW bank of electrical heating elements as well as by a chilled water heat exchanger. The mainstream air was then of uniform temperature entering the test section. At the entrance to the test section, a suction loop removed the boundary layer that developed upstream along the contraction walls of the tunnel. The new boundary layer that originated at the leading edge of the test plate was tripped to turbulent by a trip. Characteristics of the boundary layer at 1.3D upstream of the film cooling holes are given in Table 3-1 [15].

The wind tunnel facility was designed to achieve a density ratio as high as 1.8, and did so by cooling the coolant air to cryogenic temperatures similar to Pietryzk [16]. Coolant air for the film cooling injection was diverted from the mainstream flow by a 60Hz variable frequency blower that was hermetically sealed. The coolant air was sent through solid desiccant to dry the air before cooling to cryogenic temperatures. Drying the air before cooling it to cryogenic temperatures was crucial, to avoid freezing of condensate. Downstream of the desiccant, the coolant air passed through a heat exchanger cooled by liquid nitrogen, which was mixed directly into the coolant flow. Downstream of the heat exchanger, the coolant flow rate was measured by a Venturi flow meter. Thermocouples measured the temperature of the coolant flow just upstream and downstream of the Venturi flow meter so that mass flow rate could be accurately measured. The flow then entered a plenum. The interior of the plenum contained a splash plate and three conditioning screens that ensured uniformity before the flow reached the inlet to the film cooling holes.

Table 3-1. Boundary Layer Characteristics [15]

θ/D	δ/D	Re_θ	Re^*
0.13	1.2	670	315

Film cooling holes were machined out of Dow STYROFOAM™ brand residential sheathing to provide a nearly adiabatic surface ($k = 0.029 \text{ W/m}\cdot\text{K}$). Table 3-2 fully describes the geometry of the cylindrical holes tested in the current study. While there are multiple industrial processes that apply TBC to an airfoil, the current study made use of an air-plasma spray (APS) process much like that presented by Bunker [12]. This process was chosen due to the line-of-sight manner in which the process coats the surface.

The simulated TBC coating in the test coupons was sprayed by atomizing a DAPtex® Plus Multi-Purpose Foam Sealant ($k = 0.036 \text{ W/m}\cdot\text{K}$). A custom nozzle was constructed to atomize the foam sealant and spray the coating. The nozzle was made from Dow STYROFOAM™. A schematic of the nozzle is shown in Figure 3-3a. Compressed air was fed into the back of the nozzle and mixed with the foam sealant at the exit of the nozzle. It was very important to mix the air with the foam sealant near the exit of the nozzle. The compressed air was at a high pressure at the inlet to the nozzle, and experienced a large pressure drop across the length of the nozzle. The foam sealant was not at a high pressure, so it had to be mixed with the

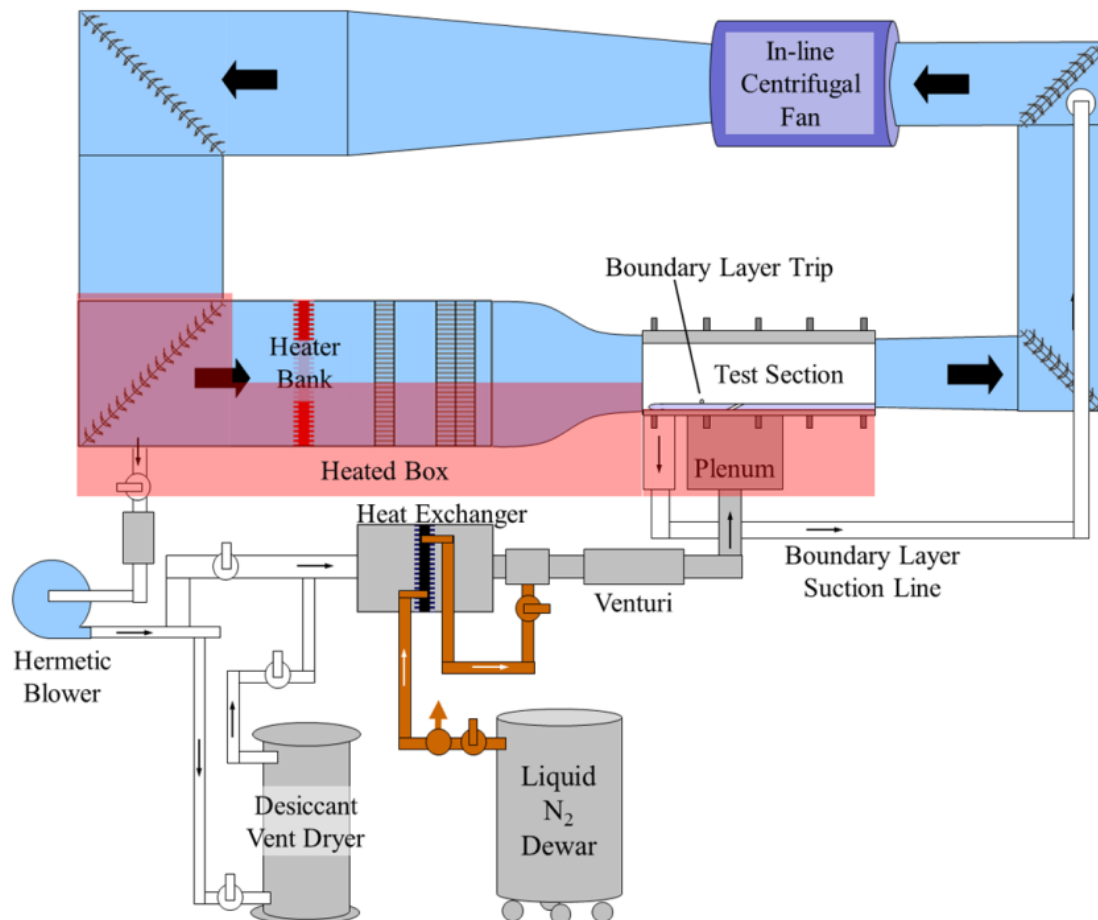


Figure 3-1. Schematic of wind tunnel used in the current study.

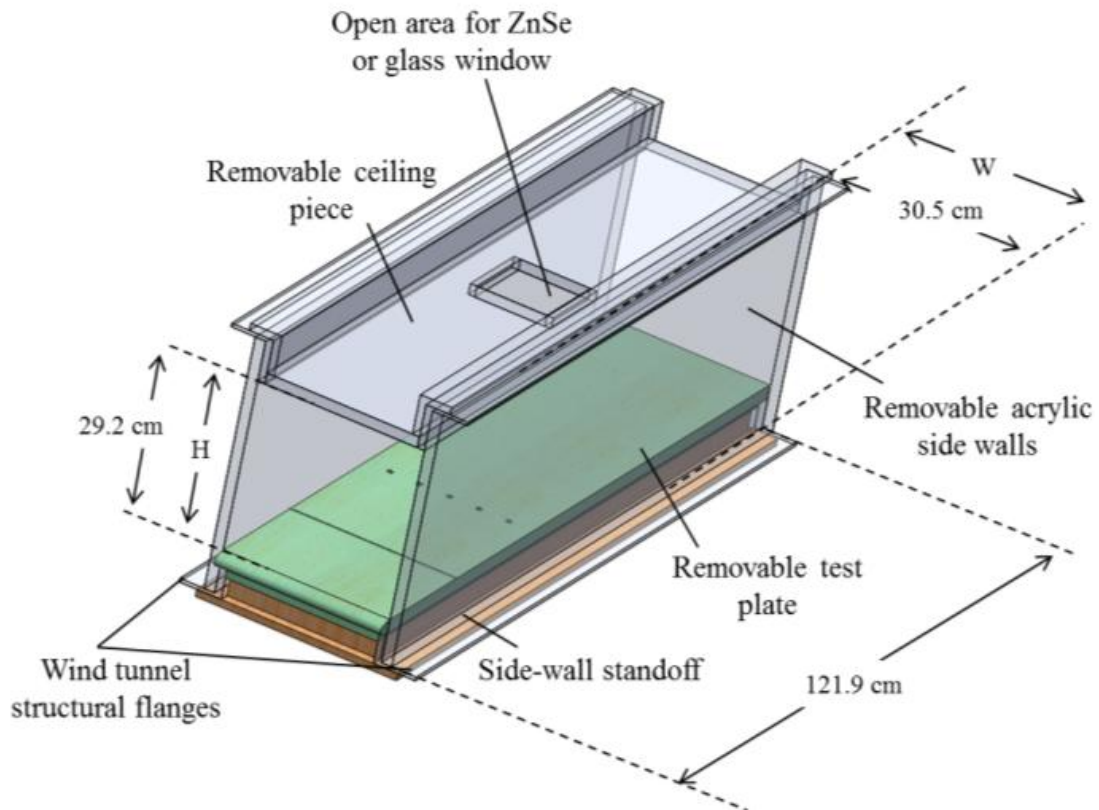


Figure 3-2. Schematic of the test section [15].

air at a location where the air pressure was low enough for the foam to flow. Many nozzles were made before settling in on a design that worked.

Figure 3-3b shows a photograph of the nozzle. A valve and pressure gage just upstream of the nozzle allowed the pressure to be set at a constant value (typically ~140 kPa) at the inlet of the nozzle. The nozzle was held about 0.5 m from the surface of the plate when the foam sealant was sprayed. After each coating was sprayed, the internal passages of the nozzle were cleaned with a pipe cleaner while the foam sealant was still wet.

Table 3-2. Description of Cylindrical Holes

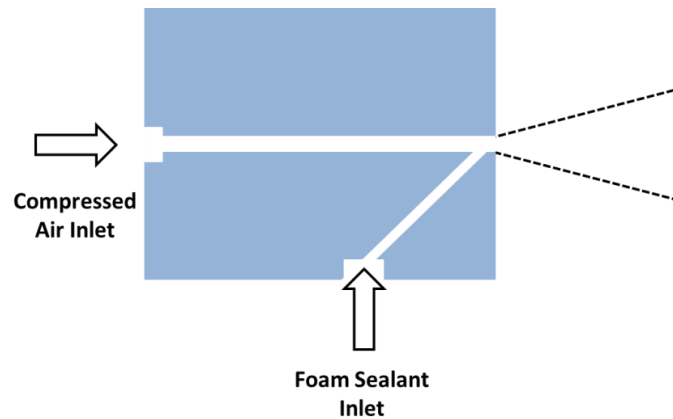
Hole Type	α	L/D	P/D	w/P	AR	D
Cylindrical	30°	4.7	6.67	0.15	1	8.2 mm

During the application process, the entire surface of the test plate, except the hole breakouts, was masked. The spray was applied perpendicular to the surface of the plate to ensure that the spray

deposited in film cooling holes in a realistic and repeatable pattern. After spraying, excess foam was scraped from the plate such that the top surface of blockages was flush with the test surface. After the foam sealant dried, the mask was removed. A photograph showing the blockage in the hole is shown in Figure 3-4. The foam was then painted black after the blockages were sprayed, such that the emissivity of the blockage was the same as the material underneath.

A cross section of a cylindrical hole was cut and the photograph is shown in Figure 3-5. The thicknesses of the deposits were estimated using geometrical relationships and verified after the coupon was removed. The thickness of the coating, t , was estimated by equation 2-1.

$$t = c * \sin(\alpha) \quad (2-1)$$



(a)



(b)

Figure 3-3. (a) Schematic and (b) photograph of nozzle for atomizing and spraying foam

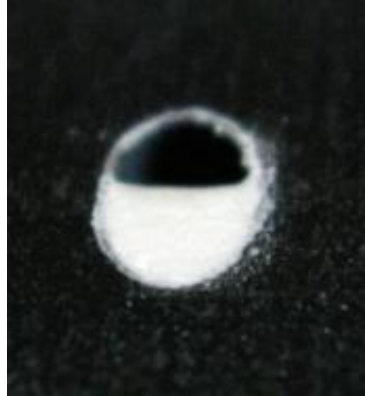


Figure 3-4. Photograph looking into a cylindrical hole with a $t/D=0.5$ blockage.

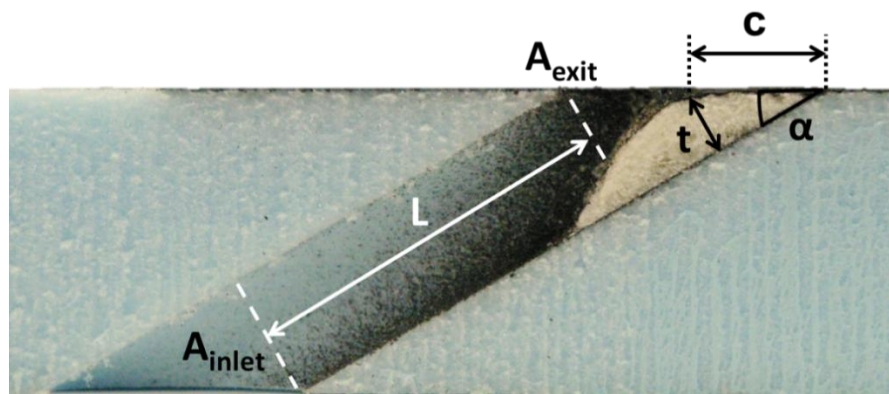


Figure 3-5. A cross-sectional photograph of a sprayed hole.

Table 3-3 displays blockage configurations used in the current study. The blockage of $t/D=0.5$ was chosen to approximately match the in-hole blockages of Demling and Bogard [8] as well as Bunker [12]. Table 3-3 also gives the effective area ratio (AR_{eff}). The AR_{eff} was meaningful, as will be shown in the results, because it was needed to determine an effective momentum-flux ratio (I_{eff}). The maximum blockage thickness was 50% of the diameter of the hole; however, the thickness of the blockage at the exit plane was smaller than the maximum blockage thickness so that only 35% of the exit of the hole was blocked.

For configurations where the exit area equaled the inlet area, $AR_{eff} = 1$ and $I_{eff} = I$ in the metering section. Blocked holes had a higher effective momentum-flux ratio than unblocked holes at the same coolant flowrate, thus contributing to jet detachment for blocked holes.

Table 3-3. Configurations of Simulated TBC Coating Tested

t_{Max}/D	AR_{eff}	Change in Exit Area From Unblocked	Location of Effective Throat
Unblocked	1	-	Anywhere in Hole
0.5	0.65	-35%	Exit

Adiabatic effectiveness measurements were determined from surface temperature measurements made with a FLIR SC620 Infrared (IR) camera. The operational temperature range of the IR camera was -40°C to 120°C ; however, coolant temperatures for $DR = 1.5$ tests were as low as -80°C . Settings in the camera's software were manually adjusted such that they would never predict temperatures lower than -40°C , and a calibration then corrected the output of the IR camera to values measured by thermocouples.

A calibration procedure was developed similar to Eberly and Thole [15] that compared temperatures measured by the IR camera to temperatures measured by thermocouples. Thermocouples adhered to small slabs of copper (1cm x 1cm x 2mm) by thermally conductive epoxy were placed on the surface of the test plate. The thermocouples were adhered to copper so that there was a large isothermal area at a known temperature (measured by the thermocouple) for the IR camera to measure. Temperatures were recorded by the thermocouples on the surface of the test plate and by the IR camera while the temperature of the copper was varied. Temperatures read by the thermocouples were plotted along with temperatures read by the IR camera, and a best fit curve was generated. Separate calibration curves were generated for each density ratio. A $DR = 1.5$ calibration curve is shown in Figure 3-6. All data taken during adiabatic effectiveness tests was corrected by this calibration curve.

Coolant and freestream temperatures were each measured using multiple thermocouples. These measurements along with the corrected IR camera measurements allowed the adiabatic effectiveness to be measured.

Pressure measurements were also made to evaluate the discharge coefficients for the unblocked and blocked cooling holes. Pressure measurements were taken in the coolant plenum as well as the mainstream using static pressure taps.

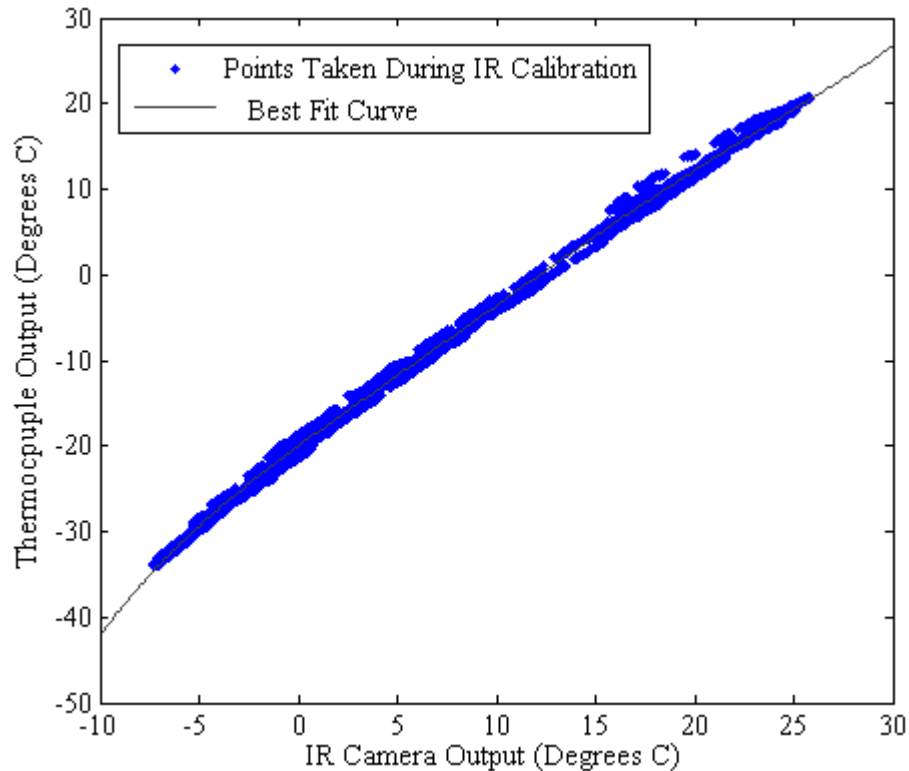


Figure 3-6. A sample DR = 1.5 calibration curve.

2.1 Uncertainty Analysis

Uncertainty calculations were performed for the flat plate effectiveness studies. A 95% confidence level was used for all uncertainty measurements. Uncertainties in density ratio and adiabatic effectiveness were found using the propagation of error method described in Figliola and Beasley [17]. Error for adiabatic effectiveness was dominated by the bias error of the thermocouples and the scatter of the calibration, and takes the value $\eta = \pm 0.019$ at high density ratio and $\eta = \pm 0.022$ at low density ratio. These uncertainty values are for the highest values of η found on the plate, and decrease to $\eta = \pm 0.010$ at the lowest values of η found on the plate for high density ratio tests. Uncertainty in density ratio was also dominated by the bias error of the thermocouples and was found to be $DR = \pm 0.3\%$ for both high and low density ratio.

Uncertainty values in blowing ratio and momentum flux ratio were mainly due to the bias error of the Venturi flow meter, which had a bias error of $\pm 0.25\%$ of the full scale reading. This value was verified by a laminar flow element connected in series with the Venturi flow meter. At

the lowest blowing ratios, the uncertainty of the Setra Model 390 pressure transducers was the largest contributor to uncertainty. Uncertainty in blowing ratio was $M = \pm 25\%$ at the lowest blowing ratio tested ($M = 0.26$). At $M = 0.5$, this value quickly dropped to $\pm 9\%$ due to a larger reading on the pressure transducer. At the highest blowing ratio tested in the current study of $M = 1.0$, the value of uncertainty was $\pm 5\%$. Uncertainty values of discharge coefficient were identical to values reported for M , due to the proportional nature of blowing ratio and discharge coefficient at incompressible flow conditions.

Uncertainty in the effective area ratio of the hole was found by cutting cross sections of the holes and directly measuring the inlet and exit areas. The uncertainty in AR_{eff} was found to be ± 0.024 . The effective momentum flux ratio has a value of $I_{\text{eff}} = \pm 19\%$ at $M = 0.5$, and $I_{\text{eff}} = \pm 10\%$ at $M = 1.0$. A more detailed explanation of the uncertainty can be found in the Appendix.

Chapter 4

Effects of Blockages on Film Cooling Holes

This chapter describes the results of adiabatic effectiveness tests run on unblocked and blocked cylindrical film cooling holes. The blockage effects on the discharge coefficients of film cooling holes will be described first. Then the effects of blockages on the adiabatic effectiveness of film cooling holes will be shown. Unblocked holes will be compared to blocked holes both at matched blowing ratio and pressure ratio. Adiabatic effectiveness results will then be scaled by the momentum flux ratio at the exit of the hole.

4.1 Blockage Effects on Discharge Coefficient

Incompressible discharge coefficients (C_d) were calculated based on the measured pressures for each $DR = 1.5$ test performed. Comparisons were made to the literature for the baseline case of a cylindrical hole with no blockage. Figure 4-1 shows discharge coefficients for holes in the current study, as well as Mensch and Thole [18], Burd and Simon [19], and Barringer et al. [20]. The data compares favorably with the available literature.

Figure 4-2 shows all the C_d for unblocked and blocked cooling holes as a function of the pressure ratio. Two equations defining the discharge coefficient were used (given in equations 4-1 and 4-2). The difference between the two definitions was the area in the denominator. For unblocked holes, the discharge coefficients were the same with both definitions because the inlet and minimum area were the same.

$$C_d = \frac{\dot{m}_{\text{actual}}}{A_{\text{min}} \sqrt{2\rho_c * \Delta P_{\text{holes}}}} \quad (4-1)$$

$$C_d = \frac{\dot{m}_{\text{actual}}}{A_{\text{inlet}} \sqrt{2\rho_c * \Delta P_{\text{holes}}}} \quad (4-2)$$

For the case with holes having a blockage, there was no more than a 10% drop in C_d due to the blockage, when C_d was defined with equation 4-2. Defining C_d with equation 4-1 instead, the discharge coefficients dropped 40% from unblocked holes. The density ratio did not seem to have an effect on the discharge coefficient.

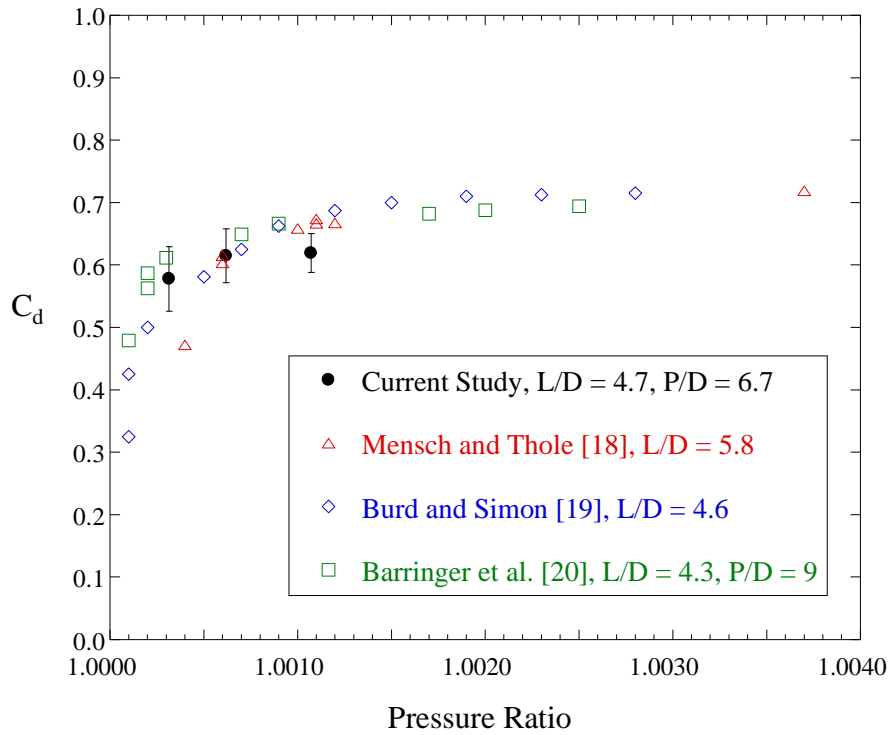


Figure 4-1. Discharge coefficients for cylindrical holes.

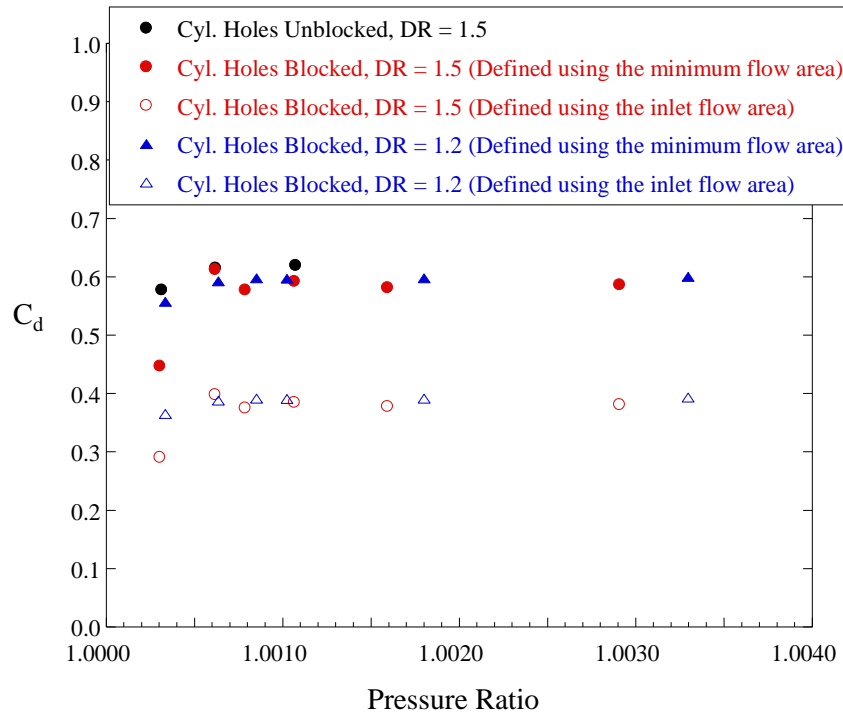


Figure 4-2. Discharge coefficients for unblocked and blocked holes.

4.2 Blockage Effects on Adiabatic Effectiveness

Adiabatic effectiveness measurements for unblocked holes were compared to those in open literature. Laterally averaged effectiveness values across three pitches are shown in Figure 4-3 for $M = 0.5$ and 1.0 as compared to data taken by Eberly and Thole [15] and Schmidt et al. [21]. The laterally averaged effectiveness compared well to other widely spaced cylindrical holes in the available literature.

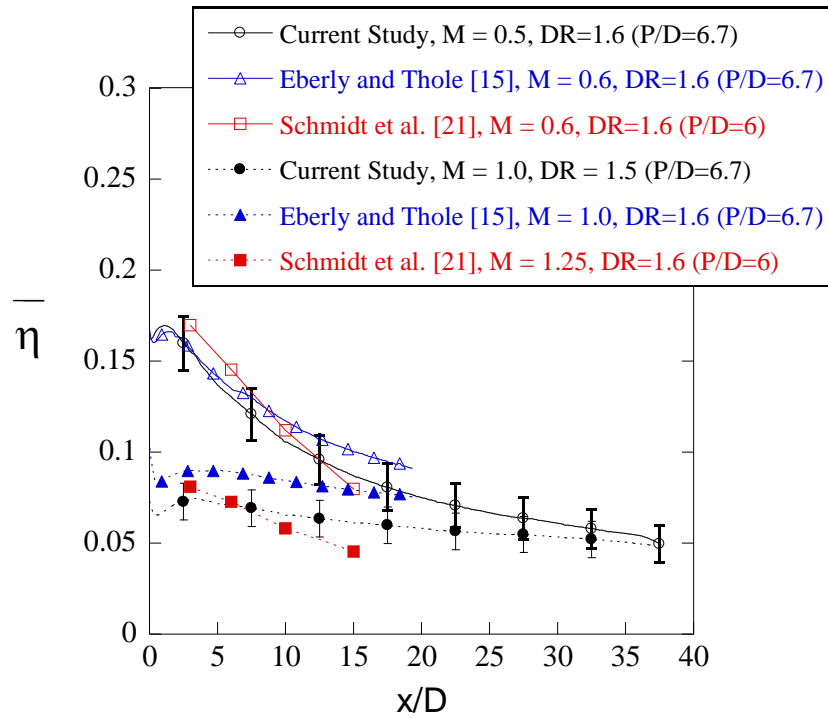
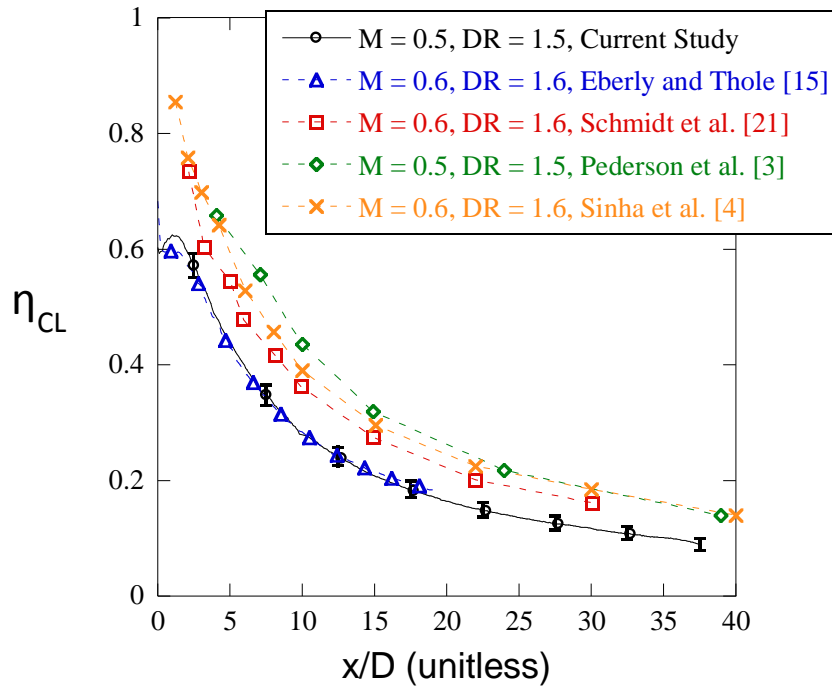


Figure 4-3. Laterally averaged effectiveness results at $M = 0.5$ and $M = 1.0$.

Centerline effectiveness results for the current study are compared to Eberly and Thole [15], Schmidt et al. [21], Pederson et al. [3] and Sinha et al. [4] at $M = 0.5$ and 0.6 in Figure 4-4. All results in Figure 4-4 are for density ratios between 1.5 and 1.6. The centerline effectiveness in the current study nearly exactly matched that of Eberly and Thole, and compared favorably to Schmidt et al., Pederson et al., and Sinha et al. The centerline and laterally averaged effectiveness values both compared well to values found in available literature. The geometry and flow conditions of the holes used in both the centerline and laterally averaged comparisons can be found in Table 4-1.

Table 4-1. Comparison of Geometry and Flow Conditions for Cylindrical Holes

Study	P/D	L/D	α (°)	DR	M	I
Current Study	6.7	4.7	30	1.5	0.5	0.18
				1.5	1.0	0.70
Eberly and Thole [15]	6.7	4.7	30	1.6	0.6	0.21
				1.6	1.0	0.64
Schmidt et al. [21]	6	4	35	1.6	0.60	0.23
					1.25	0.98
Pederson et al. [3]	3	40	35	1.5	0.52	0.17
Sinha et al. [4]	3	1.8	35	1.6	0.57	0.21

**Figure 4-4. Centerline effectiveness results at M = 0.5.**

The experimental test matrix for the current study is given in Table 4-2. As stated previously, blocked holes were tested at matched blowing ratios and pressure ratios. Three unblocked blowing ratios were tested for DR = 1.2 and DR = 1.5. Two blocked tests were performed for each unblocked test for a total of 6 tests per density ratio. Table 4-2 also lists the pressure ratio and momentum flux ratio evaluated at the exit of the hole along with the blowing ratio of each test.

Table 4-2. Blowing and Momentum Flux Ratios Tested in the Current Study

Density Ratio	Unblocked			Blocked Matched-PR			Blocked Matched-M		
	M	PR	I_{eff}	M	PR	I_{eff}	M	PR	I_{eff}
DR = 1.2	0.51	1.0003	0.22	0.29	1.0003	0.87	0.50	1.0009	0.43
	0.72	1.0007	0.17	0.44	1.0006	0.61	0.74	1.0018	0.39
	1.03	1.0011	0.50	0.56	1.0010	1.99	1.00	1.0033	1.09
DR = 1.5	0.53	1.0003	0.18	0.26	1.0003	0.70	0.53	1.0008	0.39
	0.78	1.0006	0.12	0.51	1.0006	0.74	0.75	1.0016	0.39
	1.03	1.0011	0.52	0.63	1.0011	1.95	1.02	1.0029	0.90

Figure 4-5 through Figure 4-13 present adiabatic effectiveness levels for the unblocked hole along with those of a blocked pressure ratio for three different blowing ratios. It is important to note that the matched pressure ratio cases had much lower blowing ratios than the unblocked cases, which followed from the decreases in discharge coefficients discussed previously. The matched pressure ratio cases, however, were representative of what would occur in an engine since the pressure ratio across the holes was a constant.

Figure 4-5 and Figure 4-6 show adiabatic effectiveness contours for $M = 0.5$ at DR = 1.5 and DR = 1.2, respectively. Figure 4-5a displays the unblocked hole effectiveness results, Figure 4-5b displays the blocked hole effectiveness results at matched pressure ratio, and Figure 4-5c displays the blocked hole effectiveness results at matched blowing ratio. Figure 4-5a and Figure 4-5b show decreased adiabatic effectiveness at DR = 1.5 for blocked holes at matched pressure ratio compared to unblocked holes. Very similar results were found at DR = 1.2, and can be seen in Figure 4-6a and Figure 4-6b. A drop in discharge coefficient due to the blockage lead to a large drop in flowrate ($M = 0.26$ vs. $M = 0.53$ at DR = 1.5, and $M = 0.29$ vs. $M = 0.51$ at

DR = 1.2). This decrease in flowrate contributed to the large drop in adiabatic effectiveness between the unblocked and blocked tests. An even larger drop in effectiveness was seen when comparing unblocked holes to blocked holes at matched blowing ratio (Figure 4-5a vs. Figure 4-5c at DR = 1.5, and Figure 4-6a vs. Figure 4-6c at DR = 1.2). The flowrate of coolant through the holes was the same between at $M = 0.5$, but the blocked holes experienced jet detachment. This jet detachment was driven by the increased momentum of the coolant at the exit of the hole. Blocked holes at matched blowing ratio had effective momentum flux ratios of 0.50 or greater. All unblocked tests and matched pressure ratio tests had I_{eff} values below 0.4, the value attributed to the onset of detachment by Thole et al. [5].

Centerline and laterally averaged effectiveness decays are shown in Figure 4-7a and Figure 4-7b, respectively. The general trends seen in the contours were also visible here. The unblocked holes performed better than blocked holes at either matched blowing or pressure ratio. The decrease in coolant flow of blocked holes at matched pressure ratio lowered the effectiveness at the surface compared to unblocked holes. The blocked holes at matched pressure ratio always performed better than blocked holes at matched blowing ratio, which was due to jet separation at the high momentum flux ratios seen at matched blowing ratio. The blockage decreased the exit area by 35%, thereby increasing the area averaged velocity at the exit of the coolant hole by about 54%. This 54% increase in area averaged velocity caused nearly a 140% increase in coolant jet momentum. Additionally, the centerline and laterally averaged effectiveness was higher in every case at DR = 1.5 than at DR = 1.2.

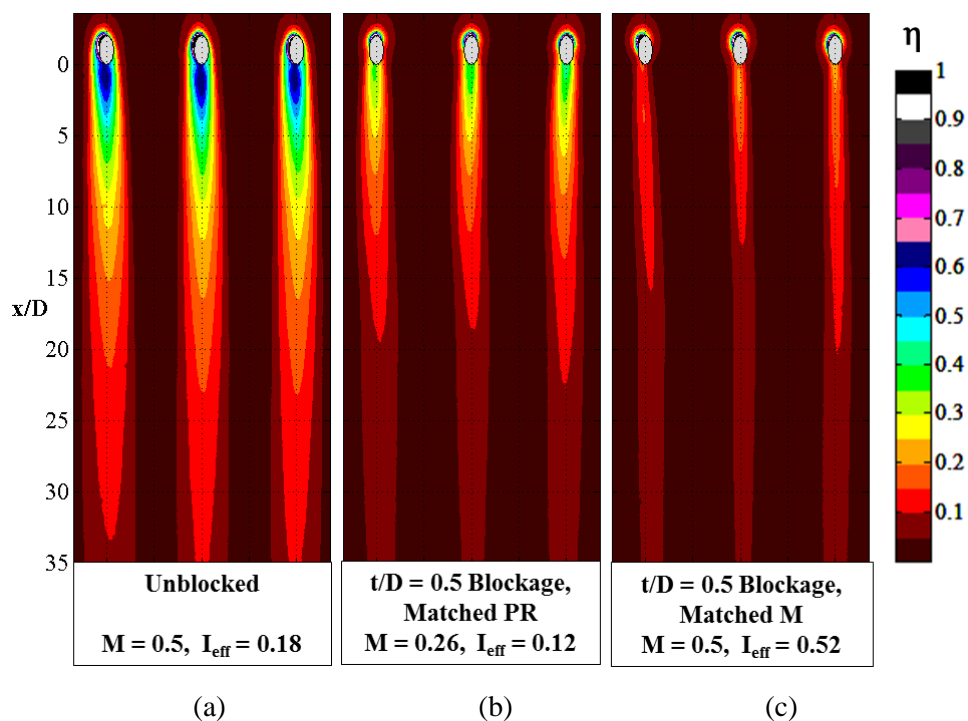


Figure 4-5. Cylindrical hole adiabatic effectiveness contours for DR=1.5 M=0.5: (a) unblocked hole, (b) blocked hole with matched PR, and (c) blocked hole with matched M.

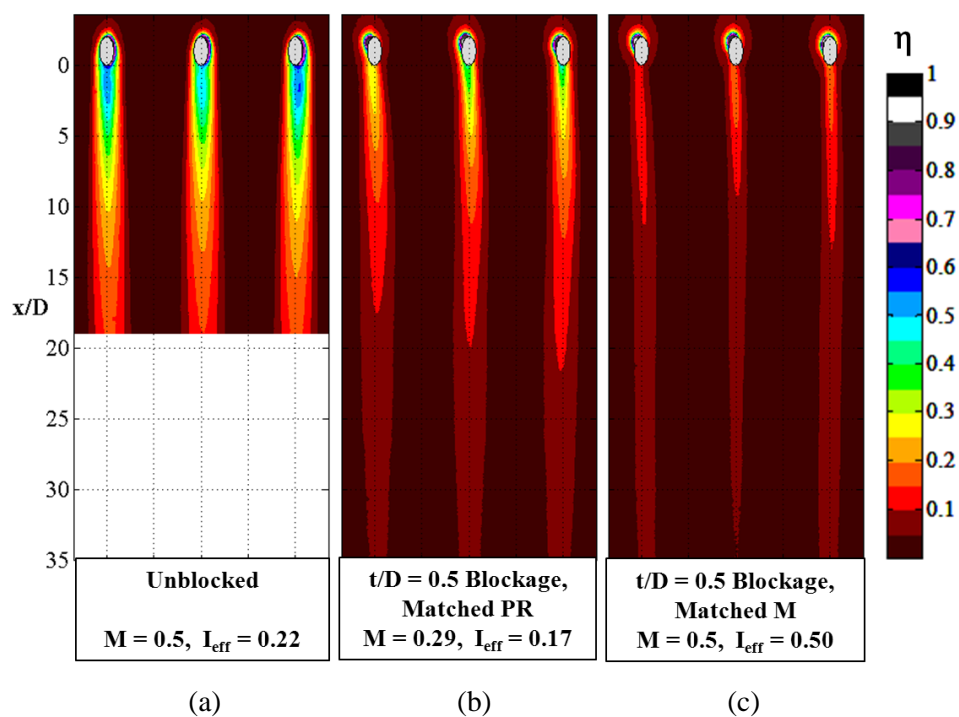


Figure 4-6. Cylindrical hole adiabatic effectiveness contours for DR=1.2 M=0.5: (a) unblocked hole, (b) blocked hole with matched PR, and (c) blocked hole with matched M.

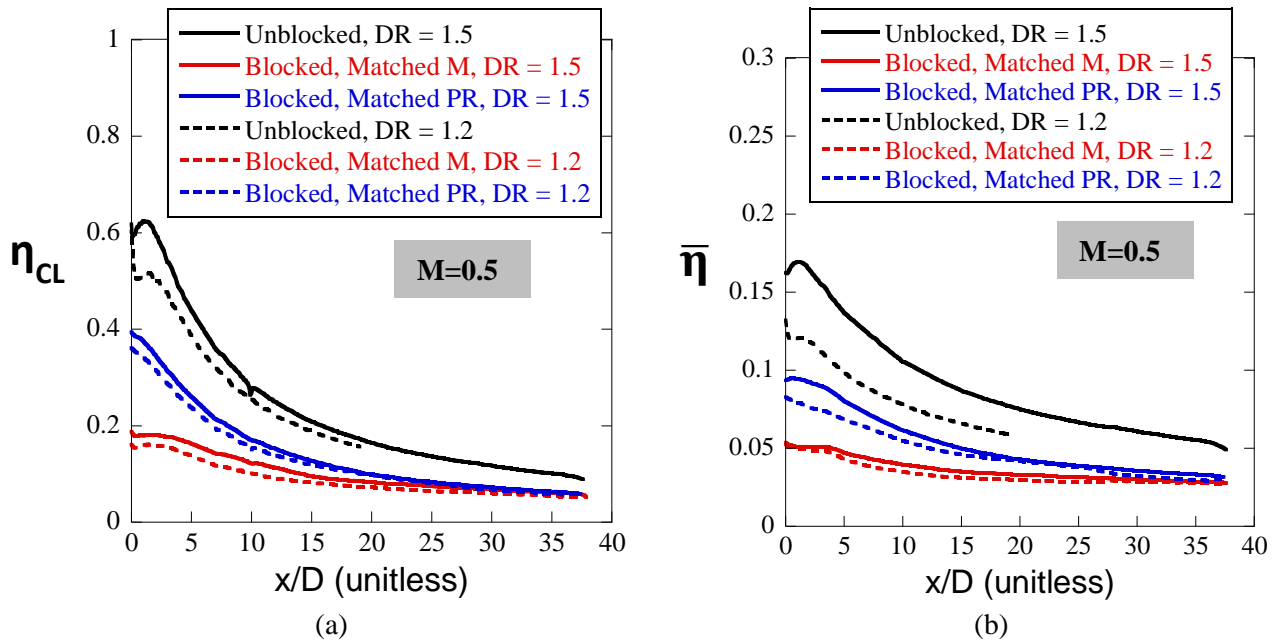


Figure 4-7. (a) Centerline and (b) laterally averaged effectiveness at $M = 0.5$, $DR = 1.5$.

Contours at $M = 0.75$ are shown for unblocked and blocked holes in Figure 4-8 for $DR = 1.5$ and Figure 4-9 for $DR = 1.2$. The trends seen in the $M = 0.75$ data were also seen in the $M = 0.5$ data. The pressure ratio matched cases showed a large decrease in effectiveness compared to unblocked tests (Figure 4-8a vs. Figure 4-8b at $DR = 1.5$ and Figure 4-9a vs. Figure 4-9b at $DR = 1.2$). Unblocked and pressure ratio matched cases had $I_{eff} \approx 0.4$, right on the border of the attached and detached-then-reattached regimes. The blowing ratio matched cases shown in Figure 4-8c and Figure 4-9c had $I_{eff} > 0.8$, meaning that it was in the fully detached range. This is visible in the contours presented in Figure 4-8c and Figure 4-9c, as past $x/D = 20$ there was no coolant present on the surface.

The centerline and laterally averaged effectiveness values show a large drop from $M = 0.5$ in Figure 4-10. The difference was most dramatic near the hole, where detachment effects were prevalent. Both blocked hole tests had very low centerline and laterally averaged effectiveness values. Figure 4-10a shows that the centerline effectiveness never exceeded 0.22 for blocked hole tests at either matched pressure or blowing ratio. Likewise, the laterally averaged effectiveness never exceeded 0.06, as shown in Figure 4-10b. The blocked hole tests showed about a 50% decrease in centerline and laterally averaged effectiveness near the hole

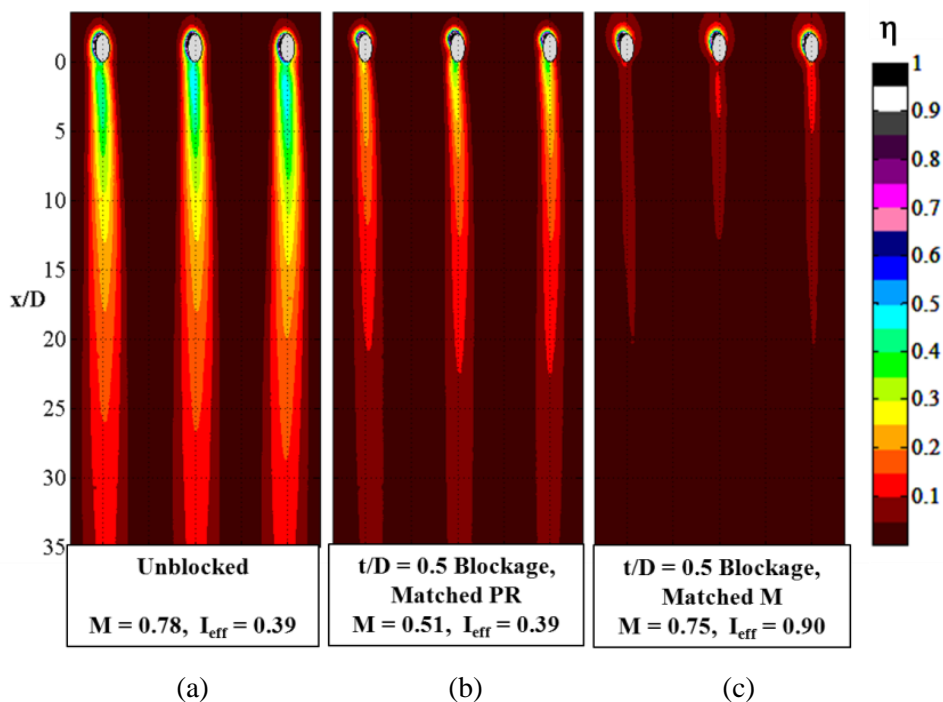


Figure 4-8. Cylindrical hole adiabatic effectiveness contours for $DR=1.5$ $M=0.75$: (a) unblocked hole, (b) blocked hole with matched PR, and (c) blocked hole with matched M.

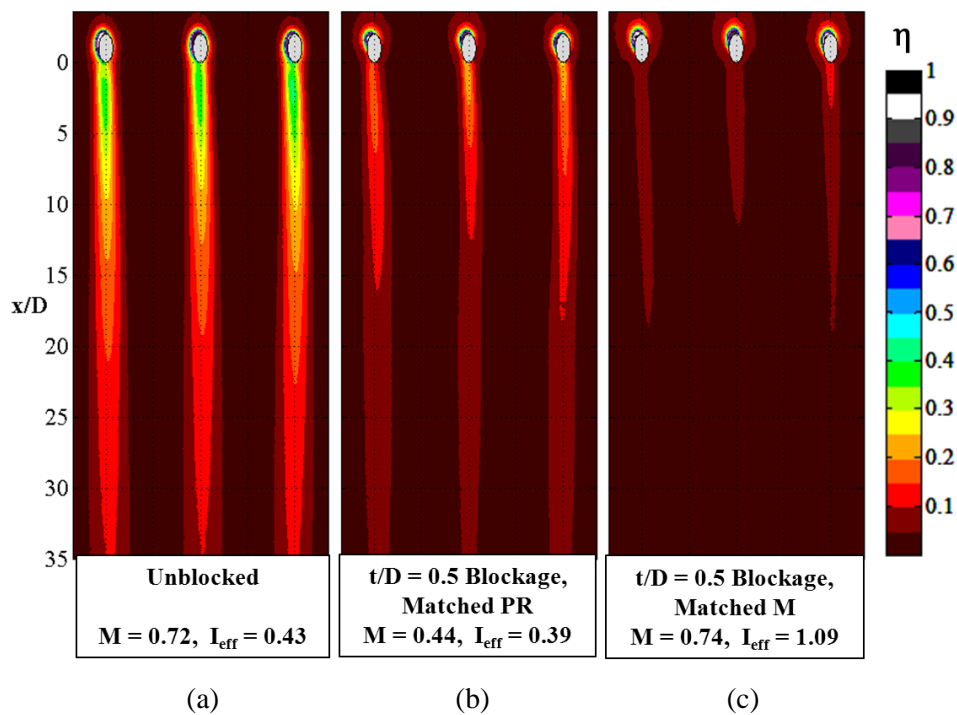


Figure 4-9. Cylindrical hole adiabatic effectiveness contours for $DR=1.2$ $M=0.75$: (a) unblocked hole, (b) blocked hole with matched PR, and (c) blocked hole with matched M.

($x/D < 10$) compared to unblocked tests. Far from the hole ($x/D > 10$), this drop in performance was closer 30%.

Unblocked hole results for $M = 0.75$ in Figure 4-10 showed higher effectiveness at $DR = 1.5$ than at $DR = 1.2$; however, blocked holes showed nearly identical effectiveness levels at $DR = 1.5$ and $DR = 1.2$. At $M = 0.5$, Figure 4-7 shows that $DR = 1.5$ results were always more effective than at $DR = 1.2$, even with blockages present. At higher blowing ratios, and therefore higher effective momentum flux ratios, blockages prevented the increased spreading of the coolant jet that was observed for unblocked holes.

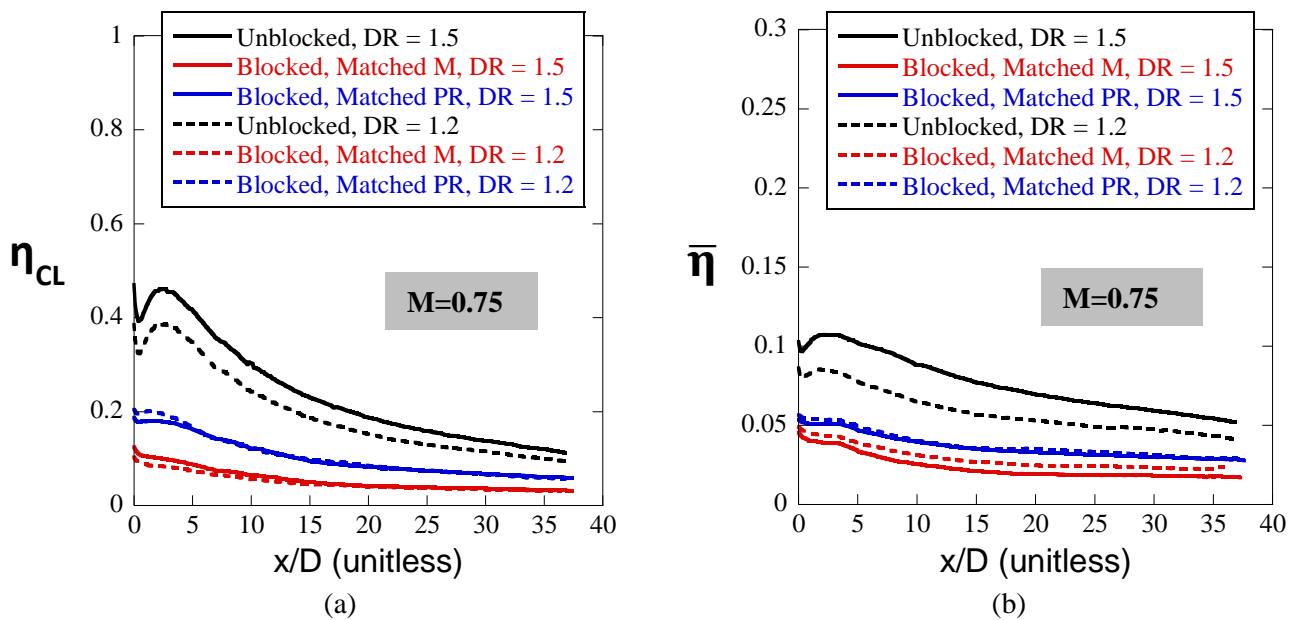


Figure 4-10. (a) Centerline and (b) laterally averaged effectiveness at $M = 0.75$, $DR = 1.5$.

Effectiveness contours at the highest blowing ratio of $M = 1$ are shown in Figure 4-11 and Figure 4-12. For this high blowing ratio case, jet detachment-then-reattachment was apparent for the unblocked cases in Figure 4-11a and Figure 4-12a. The surface coolant patterns were very narrow near the hole and widened further downstream. Matched pressure ratio cases also had this type of coolant pattern. Matched pressure ratio cases can be seen in Figure 4-11b and Figure 4-12b. All unblocked and pressure ratio matched cases had $0.4 < I_{eff} < 0.8$ (except the unblocked $DR = 1.2$ case, which had $I_{eff} = 0.87$), the range stated by Thole et al. to show detachment and reattachment [5]. The matched blowing ratio cases, shown in Figure 4-11c and Figure 4-12c, showed complete jet detachment. This detachment was so pronounced that past $x/D = 5$, almost

no coolant whatsoever saw the surface. The effective momentum flux ratios were $I_{\text{eff}} = 1.95$ and 1.99 for the $DR = 1.5$ and $DR = 1.2$ cases, respectively.

Centerline and laterally averaged effectiveness plots can be seen in Figure 4-13.

Detachment and reattachment was clearly visible for the unblocked case, seen in Figure 4-13a. The centerline effectiveness started relatively high ($\eta_{\text{cl}} = 0.45$) at the trailing edge of the hole, then decreased to a local minimum before the coolant jet reattached further downstream. There was again a large difference between the effectiveness levels of unblocked and blocked holes. The difference near the hole was 50% or more. The matched blowing ratio cases had centerline effectiveness values of below 0.15 at all x/D , and below 0.05 for all $x/D > 15$. Laterally averaged effectiveness values were $0.01 < \bar{\eta} < 0.02$.

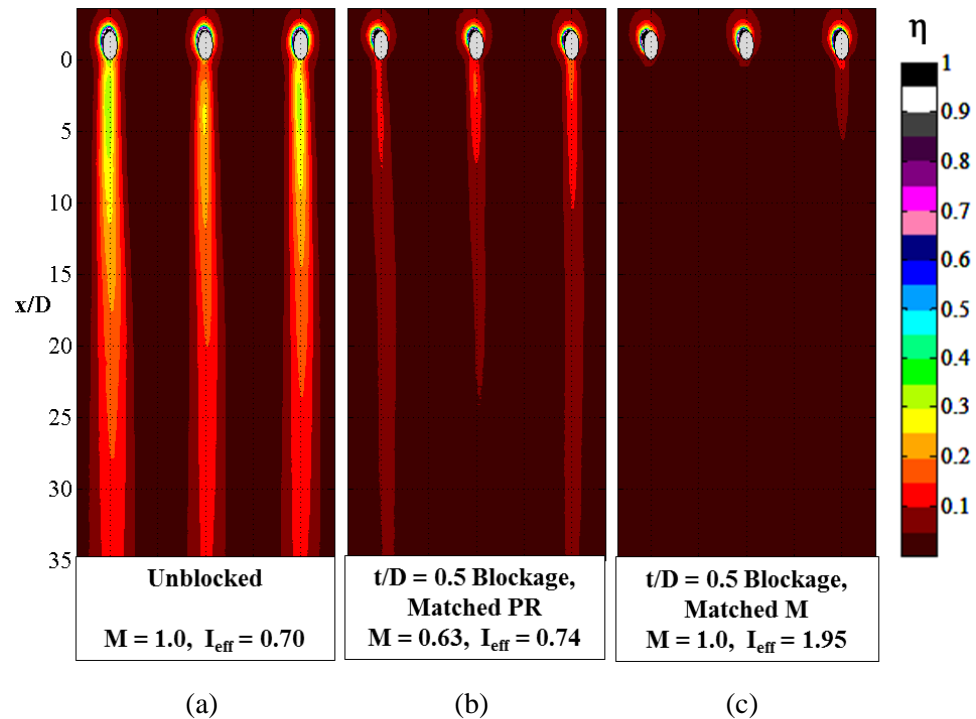


Figure 4-11. Cylindrical hole adiabatic effectiveness contours for $DR=1.5$ $M=1$: (a) unblocked hole, (b) blocked hole with matched PR, and (c) blocked hole with matched M.

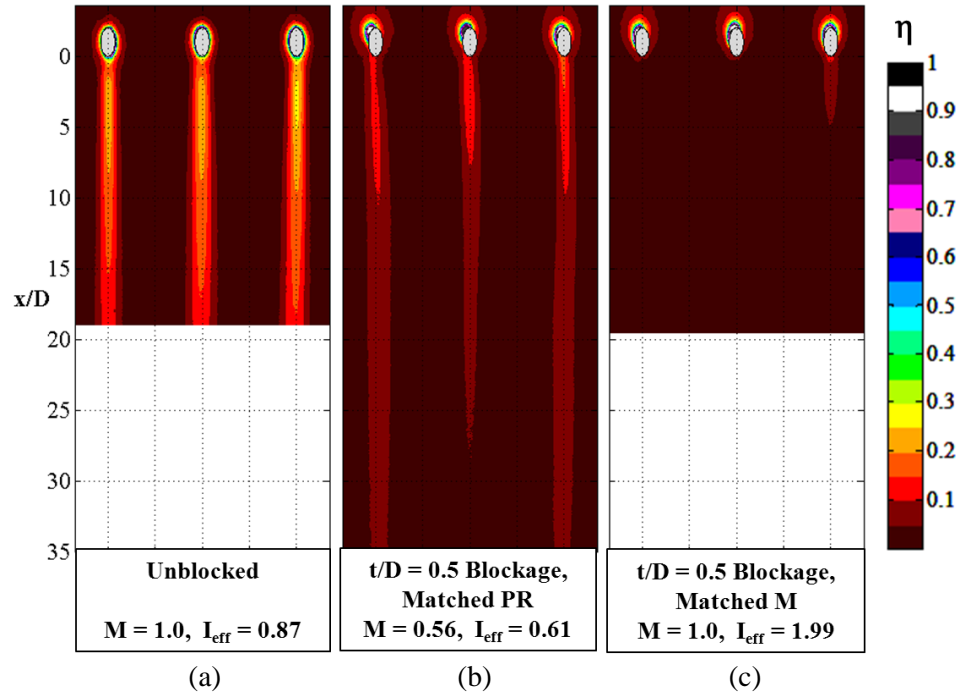


Figure 4-12. Cylindrical hole adiabatic effectiveness contours for $DR=1.2$ $M=1.0$: (a) unblocked hole, (b) blocked hole with matched PR, and (c) blocked hole with matched M.

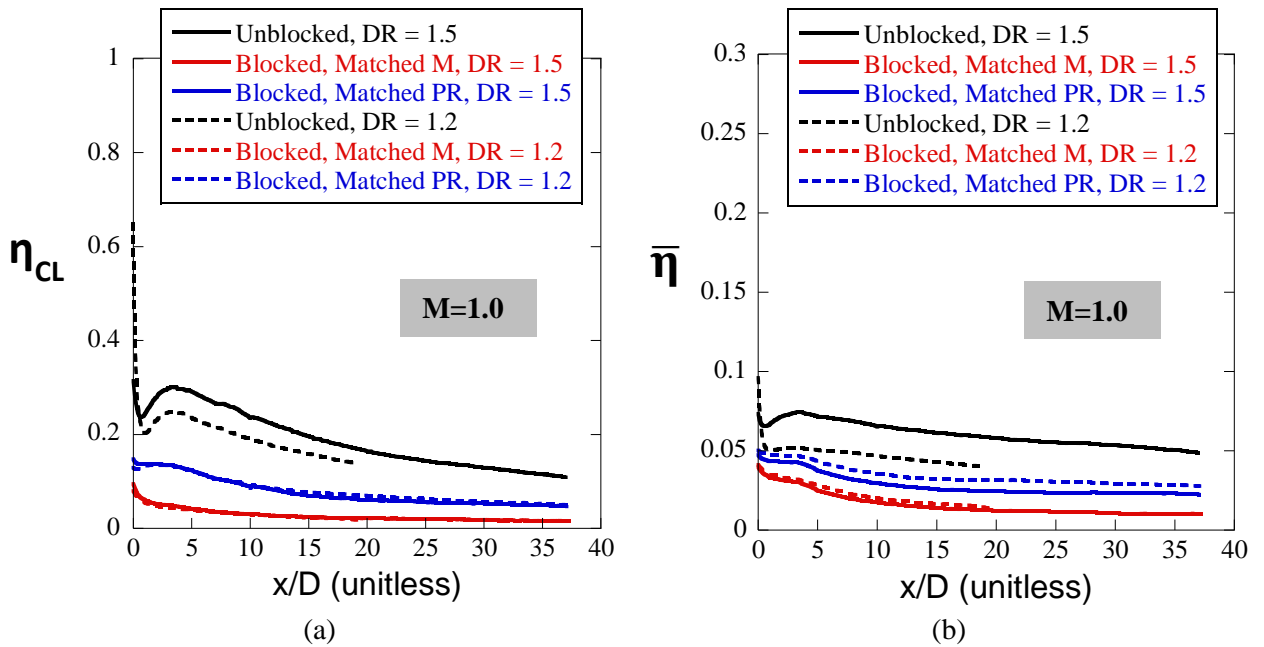


Figure 4-13. (a) Centerline and (b) laterally averaged effectiveness at $M = 1.0$, $DR = 1.2$.

Blockages prevented the spreading of coolant at $M = 1.0$ for higher density ratio cases, much like at $M = 0.75$. In Figure 4-13b, the laterally averaged effectiveness values at $DR = 1.5$ matched those at $DR = 1.2$ for blocked holes. Above $M = 0.75$, blocked hole effectiveness did not show any dependence on density ratio.

4.3 Scaling the Reduction in Adiabatic Effectiveness Due to Blockage

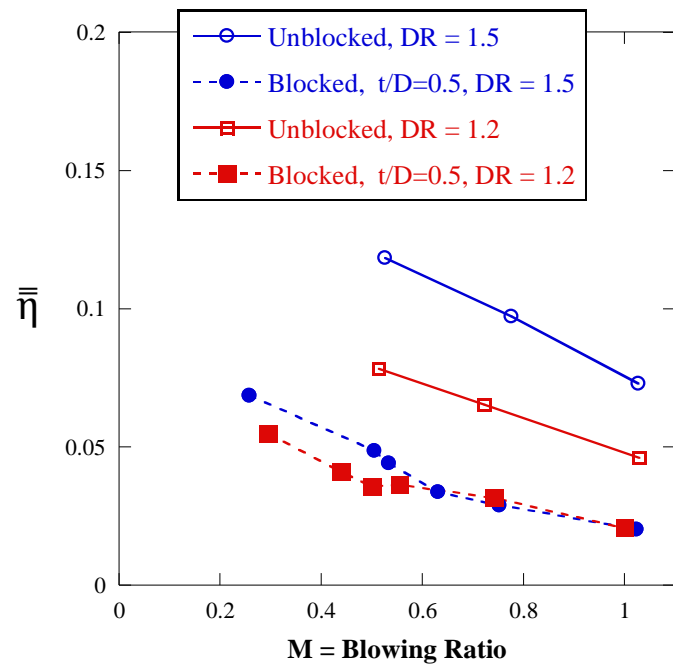
Effectiveness results were area averaged from $x/D = 3$ to 19 and plotted as a function of blowing ratio in Figure 4-14a and as a function of effective momentum flux ratio in Figure 4-14b. Three data points are present for unblocked holes ($M = 0.5, 0.75$ and 1.0), and six data points are present for blocked tests (pressure ratio matched and blowing ratio matched for the three blowing ratios). Unblocked results showed a large benefit in effectiveness for $DR = 1.5$ compared to $DR = 1.2$. This was evident in the contours, where $DR = 1.5$ results showed more lateral spreading of coolant than $DR = 1.2$ results. This trend was also observed for blocked holes, but only at low blowing ratios. Blocked hole results at blowing ratios above $M = 0.5$ did not seem to be affected by density ratio.

Unblocked results came to a peak in effectiveness at higher blowing ratios than blocked tests. Sinha et al. [4] found the highest effectiveness for unblocked cylindrical holes occurred near $M = 0.5$. By scaling with the effective momentum flux ratio instead of the blowing ratio, which is shown in Figure 4-14b, the peak effectiveness aligned for blocked and unblocked holes. Sinha et al. observed the maximum effectiveness for cylindrical holes near $I = 0.2$.

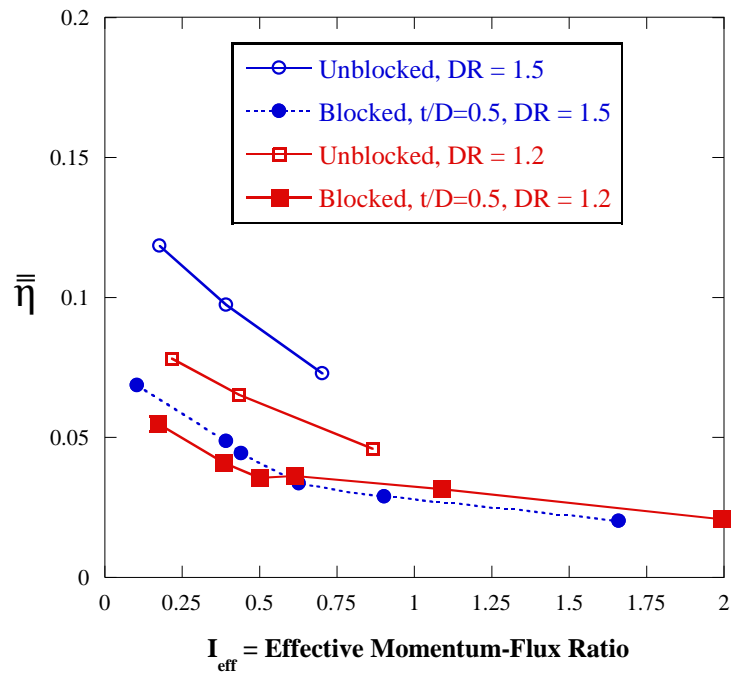
Not only did the area averaged effectiveness scale with the effective momentum flux ratio, the decrease in effectiveness also scaled with I_{eff} . Figure 4-15 shows the percent decrease in area averaged effectiveness as a function of the effective momentum flux ratio of the blocked hole test, along with data points from Demling [9] and Demling and Bogard [8]. The trendline from blockage studies performed on a shaped hole as reported by Schroeder et al. [13]. The trendline for the reduction in cooling for the shaped film cooling hole is given in Figure 4-15 for reference. The low momentum flux ratio data scaled nicely to the trendline, while the higher momentum flux ratio data tended to have more scatter. Data points corresponding to unblocked tests where I_{eff} is between 0.4 and 0.8 are marked with a dotted circle, and data where unblocked $I_{eff} > 0.8$ are marked with a solid circle in Figure 4-15. Data points where unblocked $I_{eff} < 0.4$ are not marked. The data for $I_{eff} < 0.4$ agreed well with the trend for shaped hole blockage effects as

predicted by the trendline. Data where unblocked tests exhibited detachment-then-reattachment did not always agree well with the trendline, whereas data corresponding to fully detached unblocked results never agreed with the trendline. This behavior was not seen in the shaped hole trendline because the shaped holes did not detach in the same manner as cylindrical holes.

Data from Demling [9] and Demling and Bogard [8] were taken with high freestream turbulence (~20%), while data in the current study were taken with a turbulence level of about 0.5%. High freestream turbulence tended to lift of attached jets, decreasing the effectiveness of low momentum flows. Turbulence also brought coolant back to the surface in the case of a detached jet, increasing the effectiveness of high momentum flows. Both of these effects would contribute to lower overall decreases in area averaged effectiveness.



(a)



(b)

Figure 4-14. Area averaged effectiveness plotted against (a) blowing ratio and (b) effective momentum flux ratio.

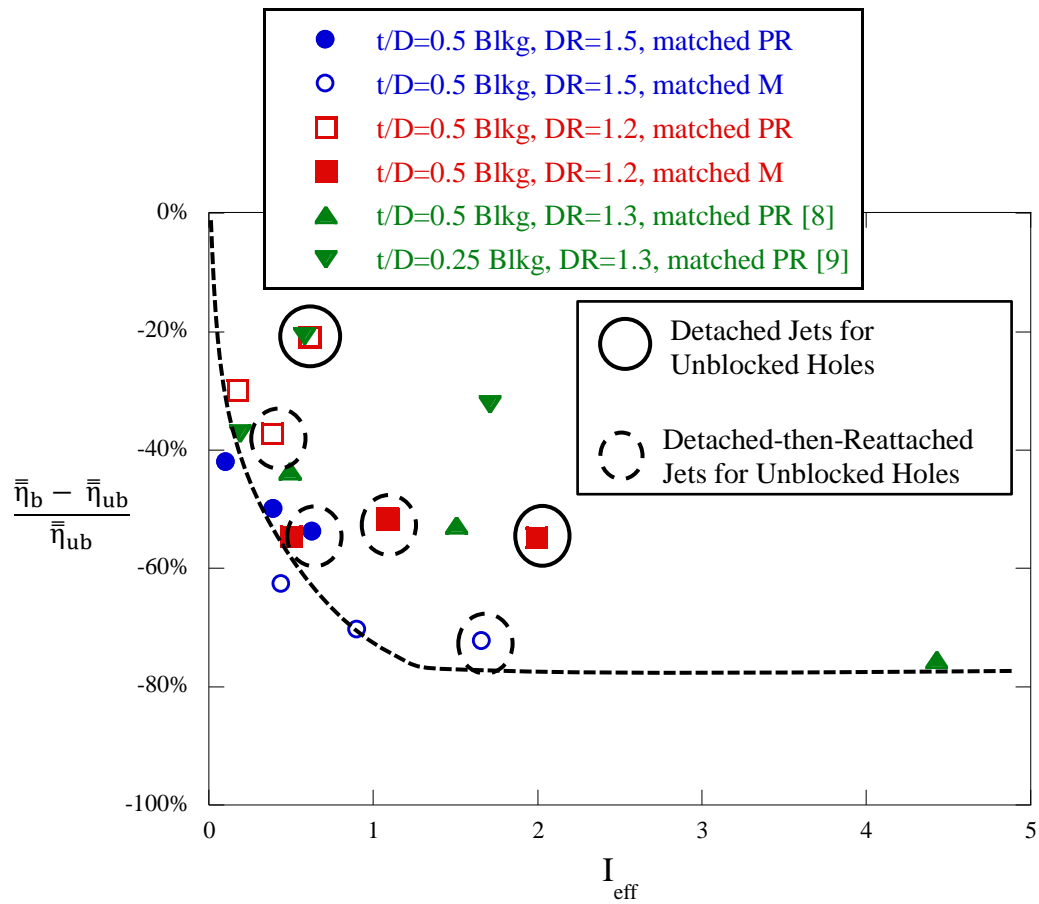


Figure 4-15. Percent change in area averaged effectiveness plotted against the effective momentum flux of the blocked hole.

Chapter 5

Conclusions

Film cooling and thermal barrier coatings are very common technologies to reduce the heat flux on turbine components as turbine inlet temperatures are increasing. The impact of applying both of these two technologies, however, is not very well studied. Only a handful of past studies have looked at the effect that blockages have on film cooling holes, while only one to the author's knowledge has used a blockage geometry similar to one that would be caused by application of a thermal barrier coating. The current study developed a method to spray a low conductivity coating on top of holes in a manner that mimicked an air-plasma spray process for actual turbine components. This study investigated cylindrical holes that were unblocked and blocked with blockage that had a maximum thickness of a half of a hole diameter.

Discharge coefficients were measured, and agreed well with literature for unblocked cylindrical holes. Discharge coefficients for the blocked holes were reported two different ways. The first method used the minimum flow area found inside the blocked holes. This resulted in discharge coefficients very similar to unblocked holes. The second method used the inlet flow area of the holes. Using this second definition of discharge coefficient, defined using the inlet area, blocked holes experienced nearly a 40% decrease in discharge coefficient from unblocked holes.

Adiabatic effectiveness tests revealed a large decrease in effectiveness due to blockages. In an actual turbine, it is expected that the supply and cooling hole exit pressure ratio remain the same and as such it was important to match the pressure ratio across the blocked cooling holes. Simulating the matched pressure ratio more accurately simulates engine conditions. In addition to the matched pressure ratio, experiments were also conducted for a matched mass flux ratio. The matched pressure ratio results showed higher adiabatic effectiveness results than for the case with the matched blowing ratio in all cases studied. The reason for this higher effectiveness level is because the matched pressure ratio resulted in lower coolant massflows and thereby lower momentum flux ratio jets. The lower momentum flux ratio jets stayed attached to the surface more so than the higher momentum flux ratio jets.

Area averaged effectiveness results for both unblocked and blocked hole tests scaled well with the effective momentum flux ratio as compared with blowing ratio. The blowing ratio, while a useful parameter to determine coolant flowrate, does not give any indication if a blockage

is present or not. The effective momentum flux ratio takes into account the effect of the blockage by incorporating the velocity at the exit of the hole. The momentum flux ratio evaluated at the interface where the jet and mainstream first mix is physically more meaningful than the blowing ratio or momentum flux ratio evaluated at the inlet of a blocked hole.

Area averaged effectiveness results seemed to come to a peak at the same I_{eff} , whether or not a blockage was present. The peak effectiveness occurred at roughly $I_{\text{eff}} \approx 0.2$. The peak effectiveness values, although occurring at the same I_{eff} , were between 30 and 40 percent higher for unblocked holes than for blocked holes. The decrease in area averaged effectiveness also scaled with the effective momentum flux ratio. As the effective momentum flux increased, the decrease in area averaged effectiveness became larger up to a 70% decrease.

A gas turbine designer could take advantage of this scaling to estimate the effectiveness of blocked film cooling holes. The designer would know the unblocked hole film effectiveness, the blockage geometry, and the pressure ratio across the hole. The flowrate of coolant through a blocked hole may be calculated by estimating the discharge coefficient of the hole. With the flowrate and the blockage size, the designer could then estimate the effective momentum flux ratio at which the blocked hole will operate. The designer would find the decrease in area averaged effectiveness in the blocked hole using the scaling with I_{eff} previously presented. Finally, the designer would be able to calculate the effectiveness of a blocked hole by multiplying the decrease in effectiveness with the unblocked effectiveness.

5.1 Recommendations for Future Work

The experiments performed in the current study only touch the surface of blockage effects on film cooling holes. Determining the sensitivity of film cooling performance on both the size and shape of blockages would be of great use to a gas turbine designer. Blockage effects for different shaped film cooling holes would also be of interest. There are many different cooling hole geometries in the literature, and it would be informative to see what effect blockages have on different hole features. Flowfield measurements using particle image velocimetry should be acquired to further understand the physics of blocked film cooling holes.

Blockages were found to increase the jet momentum at the exit of the hole, but a decrease in pristine hole area ratio would also produce the same result. A study focused on separating the effects of blockages and changes in pristine hole area ratio is recommended. Such a study would

have to be performed on shaped holes because the pristine area ratio of a cylindrical never changes.

References

- [1] Han, J.C., Dutta, S., and Ekkad, S.V., 2000, "Gas Turbine Heat Transfer and Cooling Technology", New York, New York: Taylor and Francis.
- [2] Padture, N. P., Gell, M., and Jordan E. H., 2002, "Thermal Barrier Coatings for Gas-Turbine Engine Applications," *Science* **296**, pp. 280-284
- [3] Pedersen D. R., Eckert E. R. G., and Goldstein R. J., 1977, "Film cooling with large density differences between the mainstream and the secondary fluid measured by the heat-mass transfer analogy," *ASME Transactions Journal of Heat Transfer*, **99**, pp. 620–627.
- [4] Sinha, A. K., Bogard, D. G., and Crawford, M. E., 1991, "Film Cooling Effectiveness Downstream of a Single Row of Holes With Variable Density Ratio," *J Turbomach.*, **113**(3), pp. 442-449.
- [5] Thole, K. A., Sinha, A., Bogard, D. G., and Crawford, M. E., 1992, "Mean Temperature Measurements of Jets with a Crossflow for Gas Turbine Film Cooling Application," *Rotating Machinery Transport Phenomena*, J. H. Kim and W. J. Yang, ed. Hemisphere Publishing Corporation, New York, New York.
- [6] Bogard, D.G., Schmidt, D. L., and Tabbita, M., 1998, "Characterization and Laboratory Simulation of Turbine Airfoil Surface Roughness and Associated Heat Transfer," *J Turbomach.*, **120**(2), pp. 337-342.
- [7] Jovanovic, M. B., de Lange, H. C., and van Steenhoven, A. A., 2005, "Influence of Laser Drilling Imperfection on Film Cooling Performances," *ASME International Gas Turbine Institute Turbo Expo*, Reno, GT2005-68251.
- [8] Demling, P. and Bogard, D. G., 2006, "The Effects of Obstructions on Film Cooling Effectiveness on the Suction Side of a Gas Turbine Vane," *ASME International Gas Turbine Institute Turbo Expo*, Barcelona, GT2006-90577.
- [9] Demling, P. D. R., 2005, "The Effects of Obstructions on Film Cooling Effectiveness on the Suction Side of a Gas Turbine Vane," Master's Thesis, The University of Texas at Austin.
- [10] Sundaram, N. and Thole, K. A., 2007, "Effects of Surface Deposition, Hole Blockage, and Thermal Barrier Coating Spallation on Vane Endwall Film Cooling," *J Turbomach.*, **129**(3), pp. 599-607.
- [11] Na, S., Cunha, F. J., Chyu, M. K., Shih, T. I-P., 2006 "Effects of Coating Blockage and Deposit on Film-Cooling Effectiveness and Surface Heat Transfer," *AIAA Aerospace Sciences Meeting and Exhibit*, Reno, AIAA 2006-0024.

- [12] Bunker, R. J., 2000, "Effect of Partial Coating Blockage on Film Cooling Effectiveness," International Gas Turbine and Aeroengine Congress and Exposition, Munich, 2000-GT-0244.
- [13] Schroeder, R. P. and Thole, K. A., 2014, "Adiabatic Effectiveness for an Expanded Shaped Hole at Low and High Density Ratio," ASME International Gas Turbine Institute Turbo Expo, Düsseldorf, GT2014-25992.
- [14] Whitfield, C. A., Schroeder, R. P., Thole, K. A., Lewis, S. D., 2014, "Blockage effects from simulated Thermal Barrier Coatings for Cylindrical and Shaped Cooling Holes," ASME International Gas Turbine Institute Turbo Expo, Düsseldorf, GT2014-25576.
- [15] Eberly, M. K. and Thole, K. A., 2014, "Time-Resolved Film-Cooling Flows at High and Low Density Ratios," J Turbomach., **136**(6), 061003.
- [16] Pietrzyk J. R., Bogard D. G., and Crawford M. E., 1990, "Effects of Density Ratio on the Hydrodynamics of Film Cooling," J Turbomach., **112**(3), pp. 437–443.
- [17] Figliola R. S., and Beasley D. E., 2006, Theory and Design for Mechanical Measurements, John Wiley & Sons, Inc., Hoboken, NJ.
- [18] Mensch, A. and Thole, K. A., 2014, "Overall Effectiveness of a Blade Endwall with Jet Impingement and Film Cooling," J Eng. Gas Turbines Power, **136** (3), 031901.
- [19] Burd, S. W. and Simon, T.W., 1999, "Measurements of Discharge Coefficients in Film Cooling," J Turbomach., **121**(2), pp. 243-248.
- [20] Barringer, M. D., Richard, O. T., Walter, J. P., Stitzel, S. M., and Thole, K. A., 2002, "Flow Field Simulations of a Gas Turbine Combustor," J Turbomach., **124**(3), pp. 508-516.
- [21] Schmidt D. L., Sen B., and Bogard D. G., "Film cooling with compound angle holes: Adiabatic effectiveness," J Turbomach., **118**(4), pp. 807–813.
- [22] Eberly, M. K., 2012, "Time-Resolved Studies of High Density Ratio Film-Cooling Flows," Master's Thesis, The Pennsylvania State University.

Appendix

Uncertainty Analysis

The following section further describes the methods used for calculating uncertainties using the propagation of error method as described by Figliola and Beasley [17]. Much of this section is adapted from Eberly [22], who used benchmarked this test facility.

A.1. Uncertainty in Flow Quantities

The propagation of errors in flow quantities is shown in Table A-1, starting with the measured quantities and finishing with the quantity using the most computations to arrive at. The densities of the freestream and the coolant were calculated first using the measured temperatures and pressures. A Venturi flow meter was used to calculate the volume flow rate of the coolant. For the lowest blowing ratio cases, the uncertainty in blowing ratio was dominated by the bias uncertainty of the Venturi meter, which was $\pm 0.25\%$ of the full-scale volume flow rate. This value was calculated by installing the Venturi in series with a laminar flow element and comparing the reading between the two. For the high blowing ratio cases, the bias uncertainty of the Venturi meter played a smaller role in the total uncertainty in the blowing ratio, and the uncertainty in the pressure transducer reading introduced larger error. Depending on the flow rate, different pressure transducers were used to measure the differential pressure of the Venturi. Three pressure transducers were used, all Setra model 390 transducers. The calibration of these transducers was verified by an inclined manometer. Atmospheric pressure was measured by a Setra model 370 barometer. Freestream pressure differentials were measured using a Pitot-static probe. Again, these pressure differentials were measured using Setra model 380 pressure transducers.

Table A-1. Uncertainty Progression [22]

Measured quantities	
$p_{\text{atm}}, T_{\infty}, \Delta p_{\text{pit}}$	$p_c, T_c, \Delta p_{\text{vent}}, d_c$
Calculated quantity	Propagated error
$\rho_{\infty} = \frac{p_{\infty}}{RT_{\infty}}$	$u_{\rho_{\infty}} = \left[\left(\frac{\partial \rho_{\infty}}{\partial T_{\infty}} u_{T_{\infty}} \right)^2 + \left(\frac{\partial \rho_{\infty}}{\partial p_{\infty}} u_{p_{\infty}} \right)^2 \right]^{1/2}$
$\rho_c = \frac{p_c}{RT_c}$	$u_{\rho_c} = \left[\left(\frac{\partial \rho_c}{\partial T_c} u_{T_c} \right)^2 + \left(\frac{\partial \rho_c}{\partial p_c} u_{p_c} \right)^2 \right]^{1/2}$
$U_{\infty} = \left[\frac{2\Delta p_{\text{pit}}}{\rho_{\infty}} \right]^{1/2}$	$u_{U_{\infty}} = \left[\left(\frac{\partial U_{\infty}}{\partial \rho_{\infty}} u_{\rho_{\infty}} \right)^2 + \left(\frac{\partial U_{\infty}}{\partial \Delta p_{\text{pit}}} u_{\Delta p_{\text{pit}}} \right)^2 \right]^{1/2}$
$U_c = \frac{4Q_c}{N_c d_c^2 \pi}$	$u_{U_c} = \left[\left(\frac{\partial U_c}{\partial Q_c} u_{Q_c} \right)^2 + \left(\frac{\partial U_c}{\partial d_c} u_{d_c} \right)^2 \right]^{1/2}$
$DR = \frac{\rho_c}{\rho_{\infty}}$	$u_{DR} = \left[\left(\frac{\partial DR}{\partial \rho_c} u_{\rho_c} \right)^2 + \left(\frac{\partial DR}{\partial \rho_{\infty}} u_{\rho_{\infty}} \right)^2 \right]^{1/2}$
$M = \frac{U_c \rho_c}{U_{\infty} \rho_{\infty}}$	$u_M = \left[\left(\frac{\partial M}{\partial U_c} u_{U_c} \right)^2 + \left(\frac{\partial M}{\partial \rho_c} u_{\rho_c} \right)^2 + \left(\frac{\partial M}{\partial U_{\infty}} u_{U_{\infty}} \right)^2 + \left(\frac{\partial M}{\partial \rho_{\infty}} u_{\rho_{\infty}} \right)^2 \right]^{1/2}$
$I = M \frac{U_c}{U_{\infty}}$	$u_I = \left[\left(\frac{\partial I}{\partial U_c} u_{U_c} \right)^2 + \left(\frac{\partial I}{\partial U_{\infty}} u_{U_{\infty}} \right)^2 + \left(\frac{\partial I}{\partial M} u_M \right)^2 \right]^{1/2}$

Values for bias and precision uncertainties for all of the measured quantities and the total uncertainty are given in Table A-2 for an $M = 1.0$ test and

Table A-3 for an $M = 0.5$ test, both at $DR = 1.5$. Precision uncertainty was found to be negligible in many cases because hundreds of data points were averaged.

Table A-2. Bias, Precision, and Total Uncertainties for Measured and Calculated Quantities at $M = 1.0$

	Bias	Precision	Total
$P_{\text{atm}}, \Delta P_{\text{vent}},$ ΔP_{pit} (Pa)	37	-	37
T_c (K)	1.2	0.06	1.2
Q_c (cm ³ /s)	59	-	59
d_c (mm)	0.005	-	0.005
T_∞ (K)	.35	0.06	.35
U_∞ (m/s)	0.15	-	0.15
M	-	-	0.05 (5.1% at $M = 1.0$)
I	-	-	0.07 (10% at $I = 0.70$)
DR	-	-	0.010 (0.7% at $DR = 1.5$)

Table A-3. Bias, Precision, and Total Uncertainties for Measured and Calculated Quantities at $M = 0.5$

	Bias	Precision	Total
$P_{\text{atm}}, \Delta P_{\text{vent}},$ ΔP_{pit} (Pa)	37	-	37
T_c (K)	1.2	0.06	1.2
Q_c (cm ³ /s)	59	-	59
d_c (mm)	0.005	-	0.005
T_∞ (K)	0.35	0.06	0.35
U_∞ (m/s)	0.15	-	0.15
M	-	-	0.05 (9.2% at $M = 0.5$)
I	-	-	0.03 (19% at $I = 0.19$)

A.2. Uncertainty in Adiabatic Effectiveness

The adiabatic effectiveness, calculated using Equation A-1, contains three measured temperatures: T_{∞} , T_c , and T_{aw} .

$$\eta = \frac{T_{\infty} - T_{aw}}{T_{\infty} - T_c} \quad \text{A-1}$$

The freestream temperature was measured by taking the average of four thermocouple readings in the mainstream. The coolant temperature was measured by averaging four or five thermocouple readings in the coolant plenum, just before the holes. The adiabatic wall temperature was measured as an average of five IR images corrected with a calibration equation that was calculated by comparing thermocouple and IR images over a range of temperatures. The bias uncertainty for the freestream and coolant temperature measurements was verified using an ice bath and a liquid nitrogen bath. The bias uncertainty found for the IR measurements was the difference between a thermocouple reading taken at the wall and the predicted temperature from the calibration equation at the same location. The precision uncertainties for the freestream and coolant temperatures were found to be negligible because the measurements were averaged over well over 1000 points.

Uncertainty was calculated for a particular test plate at an area of both high and low effectiveness. Additionally, a high density ratio test and a low density ratio test were both analyzed for uncertainty. Precision and bias uncertainties for the IR calibration and adiabatic effectiveness are given in Table A-4 for DR = 1.5 and Table A-5 for DR = 1.2.

Table A-4. Uncertainties for Adiabatic Effectiveness at DR = 1.5

	$\eta = 0.36$	$\eta = 0.07$
Average Temperature (°C, IR)	-3.5	19.7
TC Temperature (°C)	-14.7	10.6
TC Standard Deviation (°C)	0.09	0.08
TC Bias Uncertainty (°C)	1.2	0.35
TC Precision Uncertainty (°C)	0.06	0.06
IR Bias Uncertainty (°C)	2.6	0.39
T_{aw} Bias Uncertainty	2.9	0.53
T_{aw} Precision Uncertainty (°C)	0.95	0.27
T_{aw} Total Uncertainty (°C)	1.83	1.13
T_{∞} Uncertainty (°C)	0.35	0.35
T_c Uncertainty (°C)	1.2	1.2
η Uncertainty	0.019	0.010

Table A-5. Uncertainties for Adiabatic Effectiveness at DR = 1.2

	$\eta = 0.39$	$\eta = 0.13$
Average Temperature (°C, IR)	3.19	15.9
IR Standard Deviation	0.10	0.08
TC Temperature (°C)	1.5	15.0
TC Standard Deviation (°C)	0.13	0.05
TC Bias Uncertainty (°C)	0.35	0.35
TC Precision Uncertainty (°C)	0.03	0.03
IR Bias Uncertainty (°C)	0.04	0.04
T_{aw} Total Uncertainty (°C)	0.75	0.59
T_{∞} Uncertainty (°C)	0.35	0.35
T_c Uncertainty (°C)	0.35	0.35
η Uncertainty	0.022	0.018

For low adiabatic wall and coolant temperatures, the bias uncertainty due to the large experimental scatter when determining the calibration curve. The other uncertainties were lower because of tightened scatter about the calibration curve and lower bias uncertainties for the adiabatic wall temperature. Uncertainty estimates are conservative because of the bias uncertainty associated with the high density ratio coolant temperature (T_c). At the boiling point of liquid nitrogen, the bias uncertainty was measured to be 1.2°C; however, temperatures in the coolant were never as low as boiling liquid nitrogen, so the true bias uncertainty in T_c was likely lower 1.2°C.